JPn
Neuroscience
The Journal of Physiology

Contribution of postsynaptic T-type calcium channels to parallel fibre-Purkinje cell synaptic responses

Romain Ly[1], Guy Bouvier[1], German Szapiro[1], Haydn M. Prosser[2,6], Andrew D. Randall[2,7], Masanobu Kano[3], Kenji Sakimura[4], Philippe Isope[5], Boris Barbour[1] and Anne Feltz[1]

[1]*Ecole Normale Supérieure, Institut de Biologie de l'ENS (IBENS), CNRS UMR 8197 and INSERM U1024, Paris, France*
[2]*GlaxoSmithKline Pharmaceuticals, New Frontiers Science Park, Third Avenue, Harlow, UK*
[3]*Department of Neurophysiology, Graduate School of Medicine, University of Tokyo, Tokyo, Japan*
[4]*Department of Cellular Neurobiology, Brain Research Institute, Niigata University, Niigata, Japan*
[5]*INCI, CNRS UPR 3212, Centre de Neurochimie, Strasbourg, France*
[6]*Present address: Wellcome Trust Sanger Institute, Hinxton, Cambridge, UK*
[7]*Present address: School of Physiology and Pharmacology, Medical Sciences Building, University of Bristol, Bristol, UK*

Key points

- At the parallel fibre-Purkinje cell glutamatergic synapse, little or no Ca^{2+} entry takes place through postsynaptic neurotransmitter receptors, although postsynaptic calcium increases are clearly involved in the synaptic plasticity. Postsynaptic voltage-gated Ca^{2+} channels therefore constitute the sole rapid postsynaptic Ca^{2+} signalling mechanism, making it essential to understand how they contribute to the synaptic signalling.
- Using a selective T-type calcium channel antagonist, we describe a T-type component of the EPSC that is activated by the AMPA receptor-mediated depolarization of the spine and thus will contribute to the local calcium dynamics.
- This component can amount up to 20% of the EPSC, and this fraction is maintained even at the high frequencies sometimes encountered in sensory processing.
- Modelling based on our biophysical characterization of T-type calcium channels in Purkinje cells suggests that the brief spine EPSCs cause the activated T-type channels to deactivate rather than inactivate, enabling repetitive activation.

Abstract In the cerebellum, sensory information is conveyed to Purkinje cells (PC) via the granule cell/parallel fibre (PF) pathway. Plasticity at the PF-PC synapse is considered to be a mechanism of information storage in motor learning. The induction of synaptic plasticity in the cerebellum and elsewhere usually involves intracellular Ca^{2+} signals. Unusually, postsynaptic Ca^{2+} signalling in PF-PC spines does not involve ionotropic glutamatergic receptors because postsynaptic NMDA receptors are absent and the AMPA receptors are Ca^{2+}-impermeable; postsynaptic voltage-gated Ca^{2+} channels therefore constitute the sole rapid Ca^{2+} signalling mechanism. Low-threshold activated T-type calcium channels are present at the synapse, although their contribution to PF-PC synaptic responses is unknown. Taking advantage of 3,5-dichloro-*N*-[1-(2,2-dimethyl-tetrahydro-pyran-4-ylmethyl)-4-fluoro-piperidin-4-ylmethyl]-benzamide, a selective T-type channel antagonist, we show in the mouse that inhibition of these channels reduces PF-PC excitatory postsynaptic currents and excitatory postsynaptic potentials by 15–20%. This contribution was preserved during sparse input and repetitive activity. We characterized the biophysical properties of native T-type channels in young animals and modelled their activation during simulated dendritic excitatory postsynaptic potential waveforms. The comparison of modelled and observed synaptic responses suggests that T-type channels only activate in spines that are strongly depolarized by their synaptic input, a process requiring a high spine neck resistance. This brief and local activation ensures that T-type channels rapidly deactivate, thereby limiting inactivation during repetitive synaptic activity. T-type channels are therefore ideally situated to provide synaptic Ca^{2+} entry at PF-PC spines.

DOI: 10.1113/JP271623

(Received 21 September 2015; accepted after revision 1 December 2015; first published online 2 December 2015)
Corresponding authors A. Feltz: Institut de Biologie de l'ENS, IBENS, 46 rue d'Ulm, 75005 Paris, France. Email: anne.feltz@ens.fr

Abbreviations AHP, after-hyperpolarization; AMPAR, AMPA receptor; BBS, bicarbonate buffered solution; CGP55845, (2S)-3-([(1S)-1-(3,4-dichlorophenyl)ethyl]amino-2-ydroxypropyl)(phenylmethyl)phosphinic acid; CPCCOEt, (−)-ethyl (7E)-7-hydroxyimino-1,7a-dihydrocyclopropa[b]chromene-1a-carboxylate; D-APV, 2-amino-5-phosphonovaleric acid; DPCPX, 8-cyclopentyl-1,3-dipropylxanthine; GCL, granule cells layer; I_T, T-type current; KO, knockout; mGluR1, metabotropic glutamate receptor of the subtype $mGluR_1$; ML, molecular layer; N-type channel, $Ca_V2.2$ voltage-dependent calcium channel; PC, Purkinje cell; PF, parallel fibre; PPR, paired-pulse ratio; P-type channel, $Ca_V2.1$ voltage-dependent calcium channel; R-type channel, $Ca_V2.3$ voltage-dependent calcium channel; sEPSP, simulated EPSP; SR95531, 6-imino-3-(4-methoxyphenyl)-1(6H)-pyridazinebutanoic acid hydrobromide; TTA-P2, 3,5-dichloro-*N*-[1-(2,2-dimethyl-tetrahydro-pyran-4-ylmethyl)-4-fluoro-piperidin-4-ylmethyl]-benzamide; T-type channel, Ca_V3 voltage-dependent calcium channel; VDCC, voltage-dependent calcium channel.

Introduction

The parallel fibre (PF)-Purkinje cell (PC) glutamatergic synapse plays a major role in the processing and storage of the information involved in motor control. There is a consensus that modifications of PF-PC synaptic efficacy contribute to motor learning. At this synapse, intracellular Ca^{2+} is an important signal in the induction of plasticity, as is the case at many other plastic synapses in the brain (Daniel *et al.* 1998; Coesmans *et al.* 2004; Brenowitz & Regehr, 2005; Rancz & Hausser 2006). However, the PF-PC synapse differs from many others in the repertoire of Ca^{2+} signalling mechanisms it possesses. Notably, PF-PC synapses lack functional postsynaptic NMDA receptors (Rosenmund *et al.* 1992; Momiyama *et al.* 1996; Misra *et al.* 2000) and the AMPA receptors (AMPARs), which contain GluR2 subunits, are Ca^{2+}-impermeable (Lambolez *et al.* 1992; Hausser & Roth 1997). Although a Ca^{2+} increase is triggered by metabotropic glutamatergic receptors (mGluR1) following a train of stimuli (Batchelor *et al.* 1994), little or no Ca^{2+} entry takes place through neurotransmitter receptors during shorter bursts of activity at the synapse. Fast postsynaptic Ca^{2+} signalling is thus exclusively mediated by voltage-dependent calcium channels (VDCCs) (Hartmann & Konnerth, 2005), making it crucial to understand how VDCCs contribute to synaptic signalling.

The major VDCCs in PCs are the P-type ($Ca_v2.1$) and the T-type (Ca_v3) channels. High-voltage activated P-type channels underlie the calcium spikes described by Llinas & Sugimori (1980) and are widely distributed in PC soma, dendrites and also spines (Westenbroek *et al.* 1995; Kulik *et al.* 2004). *In situ* hybridization and electrophysiological recordings suggest an expression of T-type channels in PCs (Bossu *et al.* 1989; Mouginot *et al.* 1997; Talley *et al.* 1999; Isope & Murphy 2005). These channels are strongly expressed in dendritic spines of PF synapses, as revealed by immunofluorescence and electron microscopy (Hildebrand *et al.* 2009). Using two-photon calcium imaging and knockout (KO) mice, we have recently shown that T-type currents (I_T) are activated by bursts of synaptic activity (Hildebrand *et al.* 2009). Because T-type channels have a low activation threshold, (~ –65 mV compared to ~ –45 mV for P-type channels), they can mediate Ca^{2+} entry to spines in response to subthreshold synaptic input from PFs, which is potentially important for signalling in synaptic plasticity (Ly *et al.* 2013). By their depolarizing activity, low-threshold calcium channels might also trigger activation of P-type calcium channels (Otsu *et al.* 2014).

The present study aimed to quantify the T-type channel contribution during PF-PC synaptic transmission. We show that 3,5-dichloro-*N*-[1-(2,2-dimethyl-tetrahydro-pyran-4-ylmethyl)-4-fluoro-piperidin-4-ylmethyl]-benzamide (TTA-P2), which inhibits all three T-type Ca^{2+} channel isoforms in expression systems (Shipe *et al.* 2008) and in thalamic neurons (Dreyfus *et al.* 2010), blocks the $Ca_V3.1$ current present in PCs. Taking advantage of this inhibitor, we show that T-type current (I_T) activation is responsible for significant synaptic charge during PF-PC synaptic transmission. Investigation of the kinetics and conditions of activation of T-type channels suggests that they may be recruited exclusively in spines receiving strong synaptic inputs. This mechanism could explain the surprising apparent invariance of the T-type channel contribution to PF-PC synaptic transmission.

Methods

Slice preparation and recordings

Parasagittal and coronal slices (250 or 300 μm thick) were prepared from the cerebellum of male C57BL/6 mice (7–9 days old and 16–21 days old) in accordance with Centre National de la Recherche Scientifique animal experimentation guidelines. They were cut in a protective solution mimicking the intracellular medium (Dugue *et al.* 2005). The composition was (in mM): 130 potassium gluconate, 14.6 KCl, 2 EGTA, 20 Hepes, 25 glucose, 2-amino-5-phosphonovaleric acid (D-APV) 0.05 and 0.00005 minocycline; the solution was maintained just above its freezing point. Slices were then rinsed in

a mannitol-based solution containing (in mM): 230 mannitol, 2.5 KCl, 26 $NaHCO_3$, 1.25 $NaHPO_4$, 25 glucose, 0.8 $CaCl_2$, 8 $MgCl_2$, D-APV 0.05 and 0.00005 minocycline. Finally, the slices were allowed to equilibrate for at least 1 h at 32°C in an oxygenated (95% O_2, 5% CO_2) bicarbonate buffered solution (BBS) containing (in mM): 120 NaCl, 3 KCl, 26 $NaHCO_3$, 1.25 NaH_2PO_4, 2 $CaCl_2$, 1 $MgCl_2$ and 20 glucose (310 mosmol l^{-1}, pH 7.35) and then transferred to the recording chamber where they were perfused (>4 ml min^{-1}) continuously with BBS at 32°C. Cells with a leak current exceeding 700 pA at ∼ –63 mV were discarded. Access resistance was continuously monitored by measuring responses to 2 or 4 mV hyperpolarizing pulses from the holding potential. Cells with more than 20% change in series resistance were rejected. The series resistance was always compensated by >75%. In current clamp, the bridge was balanced and optimal capacitance neutralization applied. Data were low-pass filtered at 2.7 kHz using the built-in Bessel filter of the amplifier and sampled at 20 or 50 kHz. Cerebellar PCs were visually identified using a Axioskop 2 microscope with an Achroplan 60× water immersion lens (Carl Zeiss, Oberkochen, Germany) and a CoolSnap HQ camera (Photometrics, Tucson, AZ, USA).

PF-PC synaptic current and potential recordings (P15–P25 mice)

For these experiments, to ensure the stability of the EPSCs, we added 10 μM 6-imino-3-(4-methoxyphenyl)-1(6H)-pyridazinebutanoic acid hydrobromide (SR95531), 1 μM (2*S*)-3-([(1*S*)-1-(3,4-dichlorophenyl)ethyl]amino-2-ydroxypropyl)(phenylmethyl)phosphinic acid (CGP55845), 200 nM 8-cyclopentyl-1,3-dipropylxanthine (DPCPX) and 50 μM (−)-ethyl (7*E*)-7-hydroxyimino-1,7a-dihydrocyclopropa[b]chromene-1a-carboxylate (CPCCOEt) to the bath solution (BBS) to block GABA-A, GABA-B, adenosine A1 and mGluR1 receptors, respectively. For the experiments evaluating the TTA-P2 effect at the same time as controlling for any possible EPSC rundown, the SR95531 concentration was lowered to 2.5 μM, CPCCOEt was omitted and 10 μM ZD 7288 was added. Patch pipettes typically had initial resistances of 2.5–3.5 MΩ when filled with an internal solution, which contained (in mM): 140 $KMeSO_4$, 6 NaCl, 2 $MgCl_2$, 10 Hepes, 4 MgATP, 0.5 Na_3GTP, 10 phosphocreatine and 0.3 EGTA adjusted to pH 7.4 with KOH 1 M, ∼300 mosmol l^{-1}. Series resistance values were between 3.5 and 7.5 MΩ, compensated by ∼80%. EPSCs were evoked by stimulating PFs extracellularly by means of a glass pipette (tip diameter 10–15 μm). The size of the stimulation electrode minimizes the effects of any drift. We also made time-lapse videos to ensure that the electrode did not move with time. The stimulation electrode was placed at the surface of the molecular or the granule cell layer (GCL) at a distance of 100 μm from the dendrite plane of the recorded PC to avoid direct stimulation of the PC itself. Stimulation intensity and duration were fixed at the beginning of the experiment (1 and 10 V at 100 μs) and remained unchanged during the experiment. Experimental protocols were only initiated after a stable baseline period of EPSC amplitudes. Illustrated traces are the average of at least three individual synaptic responses. Imposed membrane potentials are reported after correction for the 8 mV measured liquid junction potentials (the real membrane potential was more negative than that reported by the amplifier).

Isolation of T-type currents (P7–P9 animals)

Whole-cell patch clamp recordings of PCs were obtained using a Multiclamp 700B amplifier and Digidata 1322A, controlled with a computer running pCLAMP, version 10.2 (Molecular Devices, Sunnyvale, CA, USA). Patch pipettes had typical initial resistances of 3–4 MΩ when filled with an internal solution that contained (in mM): 120 CsCl, 5 TEACl, 0.5 $MgCl_2$, 10 Hepes, 4 MgATP, 0.5 Na_3GTP and 20 BAPTA, adjusted to pH 7.4 with CsOH, ∼300 mosmol l^{-1}. The solution was supplemented with a morphological dye (Alexa 488™; 200 μM). Imposed membrane potentials are reported with correction for the 3 mV liquid junction potentials measured in our recordings. Subtraction of capacitance and leak currents was performed on-line using the pCLAMP (P/6) leak subtraction protocol or off-line using custom procedures (Igor; Wavemetrics, Tigard, OR, USA). To record the PC T-type current in isolation, a number of drugs (in mM) were added to the bath (BBS) solution to block Na_V (TTX, 0.0001), K_V (4-aminopyridine, 1; tetraethyl-ammonium chloride, 5) and Ca_V (Agatoxin-TK, 0.0001; cadmium, 0.2; isradipine, 0.01) currents, as well as GABAergic transmission (Picrotoxin, 0.04; SR95531, 0.01) and the hyperpolarization-activated current I_h (CsCl, 2).

Templates for EPSP waveforms were built using exponential rising (τ_{ON}) and decay (τ_{OFF}) phases:

$$V(t) = K\left(-\exp\left(-\frac{t}{\tau_{ON}}\right) + \exp\left(-\frac{t}{\tau_{OFF}}\right)\right) \quad (1)$$

where τ_{ON} and τ_{OFF} for the four templates used were respectively, 1 and 5 ms, 2 and 5 ms, 2 and 50 ms, and 5 and 100 ms. Amplitudes were normalized by adjusting the constant *K*.

When the command was a burst of simulated EPSPs, to mimic the paired pulse facilitation observed at the PF-PC synapse, the second waveform had an increased amplitude that was frequency-dependent: the paired-pulse ratio (PPR) was 1.1, 1.5, 1.7 and 1.8 at 10, 50, 100 and 200 Hz for these ionic conditions (A. Valera and P. Isope,

personal communication); for P17–P21-day-old animals and in the presence of 2 mM Mg^{2+}, see (Valera *et al.* 2012). The three subsequent stimuli were kept at the same amplitude as the second.

Drugs

TTA-P2 [(3,5-dichloro-*N*-[1-(2,2-dimethyl-tetrahydro-pyran-4-ylmethyl)-4-fluoro-piperidin-4-ylmethyl]-benz-amide) (Merck, Darmstadt, Germany), which is compound (*S*)-5 in Shipe *et al.* (2008), was made up as a 10 mM stock solution in DMSO; aliquots were kept at –20°C until use and were diluted as indicated. For TTA-P2 selectivity assessment, radioligand binding assays were conducted at MDS Pharma Services (King of Prussia, PA, USA) in accordance with standard protocols. TTX and CPCCOEt were obtained from Tocris (Tocris Bioscience, St Louis, MO, USA) and D-APV from Ascent Scientific (Bristol, UK). All other chemicals were purchased from Sigma-Aldrich (St Louis, MO, USA).

Double KO mice

Mice lacking the *cacna1g* gene (encoding $Ca_V3.1$) were produced as described previously (Petrenko *et al.* 2007). Mice lacking the *cacna1i* gene (encoding $Ca_V3.3$) were produced as described by Astori *et al.* (2011). Cryopreserved embryos of mice lacking the *cacna1i* gene (encoding $Ca_V3.3$) were resuscitated by Charles River Laboratories (Bois des Oncins, France). Heterozygote offspring were obtained by crossing male chimaeras with C57BL/6 J females; by crossing heterozygotes, homozygote offspring were obtained. Finally, double KO mice ($\alpha1G^{-/-}$ $\alpha1I^{-/-}$) were produced by crossing the two lines. All animals were bred on C57BL6/J background and litter mate controls were used where possible.

Model

To model spine, dendritic and somatic synaptic potentials, we adapted the classic two-compartment PC model of Llano *et al.* (1991) to introduce a more realistic individual dendrite. We did this by splitting the dendritic compartment into two unequal portions that retained the characteristic dendritic time constants. This was ensured by scaling the axial resistance and membrane capacitance reciprocally (Fig. 1). We neglected the membrane conductance because it has little influence on rapid events in voltage clamp. The smaller dendritic compartment represented 1% of the dendritic tree and received input from an explicitly represented spine synapse. The spine of 1.12 μm^2 area (Harris & Stevens 1988) was equipped with AMPARs and T-type calcium channels. We also added T-type calcium channels to the dendritic compartment. We validated this choice of dendritic representation by comparing the dendritic depolarization with that in spiny branchlets in the multicompartment model of Roth & Häusser (2001). They found that a single synaptic input conductance produced a peak dendritic depolarization of a few millivolts, depending upon the position of the synaptic input in the dendritic tree. Using inputs producing similar synaptic charge, our model produced a dendritic depolarization of 8 mV, which is larger than that predicted by Roth and Häusser for nearly all input locations. Our model therefore tends to overestimate the depolarizations in spiny branchlets. However, the main conclusions from our modelling will relate to the difficulty of activating T-type calcium channels synaptically, and so a more explicit and accurate model would only reinforce our qualitative conclusions. We modelled sparse input to the PC dendritic tree as activating a single synapse on a spiny branchlet represented by the individualized dendrite described above.

The synaptic current I_{AMPA} was represented by $I_{AMPA} = N_{AMPA} \cdot g_{AMPA} \cdot (e^{-t/\tau_{ON}} - e^{-t/\tau_{OFF}}) \cdot (V - E_{AMPA})$ where g_{AMPA} is the AMPA receptor unitary conductance (10 pS) and N_{AMPA} is the number of AMPA receptors, V is the membrane potential, and E_{AMPA} is the reversal potential of AMPA receptors. The kinetic equations for T-type calcium channels were derived from electrophysiological recordings in young animals (see "T-type calcium channel biophysical properties" section) and modelled using a Hodgkin–Huxley formalism. I_T was described as $I_T = N_t \cdot g_t \cdot m^3 h(V - E_{Ca})$ where m and h are the activation and inactivation variables with derivatives $\frac{dm}{dt} = \frac{m_\infty - m}{\tau_m}$ and $\frac{dh}{dt} = \frac{h_\infty - h}{\tau_h}$. N_t and g_t are the number and the unitary conductance (2 pS) of T-type calcium channels respectively, E_{Ca} is the reversal potential of T-type calcium channels measured in our experiments.

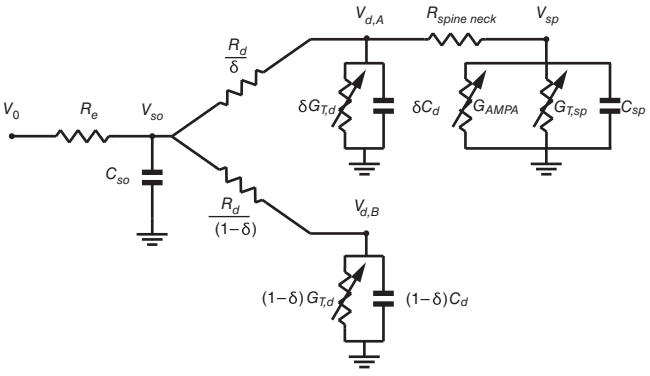

Figure 1. Circuit of the PC model
Circuit elements: *V*, potential; *R*, resistance; *C*, capacitor; G_T,G_{AMPA}, variable conductances for T-channels and AMPA receptors respectively. Locations: command potential, V_0; electrode, *e*; somatic compartment and the primary smooth dendrite, *so*; dendritic compartment with the active spine, *d, A*; passive dendritic compartment, *d, B*; spine, *sp*. δ (= 0.01) indictates the fraction of the dendritic tree receiving an active synapse.

Equations for m_∞, h_∞, τ_m and τ_h are given in the Appendix. All values used in the model are given in the Appendix. To model current clamp conditions, we added a uniform leak conductance in the soma and the dendrites (the leak reversal potential was set to the holding potential), and the electrode resistance was set to infinity; all other parameters were unchanged.

The equations of the circuit were solved numerically using the Differential Algebraic Equations solver (daspk) from the deSolve (Soetaert *et al.* 2010) package using R software (The R Project for Statistical Computing, Vienna, Austria). A ten-fold reduction of the absolute and relative tolerance parameters of the simulation produced a fractional change of 3.1×10^{-9} in the simulated EPSCs, suggesting that the simulation had converged to an accurate solution.

Data and statistical analysis

Analysis was performed with IGOR (Wavemetrics) using custom-developed macros. The PPR was measured by the ratio between peak amplitude of two consecutive responses without subtraction of the tail of the first response from the second. The synaptic charge of the second response was calculated after subtraction of the waveform of a single response. TTA-P2 inhibition was measured as the ratio between peak amplitudes after and before drug application. Data are reported as the mean ± SEM and statistical analysis was performed with GNU, version R 2.12 (R Development Core Team, 2011) and non-parametric tests were applied unless otherwise stated. Linear fits were performed using R robust regression (MASS package).

Results

TTA-P2 blocks 20% of the PF-PC EPSC

In the present study, we investigated the involvement of T-type calcium channels during synaptic transmission by using a recently developed specific inhibitor of these channels: TTA-P2. TTA-P2 has been shown to abolish the I_T generated by Cav3.1 channels in thalamo-cortical cells without affecting other voltage-dependent conductances (Dreyfus *et al.* 2010). Consistent with a lack of effect on glutamatergic EPSCs (Dreyfus *et al.* 2010), 10 μM TTA-P2 did not displace radiolabelled ionotropic glutamate receptor ligands (–8, –3, –4, –3 and 0% inhibition of 5 nM [^{3}H]-AMPA, 5 nM [^{3}H]-kainic acid, 2 nM [^{3}H] CGP-39653, 0.33 nM [^{3}H]-(((*E*)-3-(2-phenyl-2-carboxyethenyl)-4,6-dichloro-1[^{3}H]-indole-2-carboxylic acid) and 4 nM [^{3}H]-*N*-[1-(2-thienyl)cyclohexyl]-3,4-[^{3}H]piperidine binding, respectively).

We verified the efficacy and specificity of TTA-P2 inhibition of the native T-type calcium current in PCs. Cells were recorded with a pipette solution designed to isolate Ca^{2+} currents. For these experiments, we used young mice (P7–P9) to reduce space clamp errors (Isope & Murphy, 2005; Roth & Häusser, 2001). At this age, PCs develop rapidly and the dendritic surface area can vary strongly between cells in the same animal (McKay & Turner, 2005). Cells whose capacity current time constant was >800 μs were discarded. In these experiments, the peak control I_T was −220 ± 52 pA (n = 10) for a depolarization to –43 mV after a 500 ms hyperpolarizing pulse to –83 mV from a –63 mV holding potential. Bath application of 100 nM TTA-P2 led to an inhibition of 61.0 ± 0.1% of I_T within 8 min (Fig. 2*A* and *B*). This effect was concentration-dependent with an IC_{50} <100 nM and complete inhibition was attained at ∼500 nM, the concentration employed for all subsequent experiments (Fig. 2*C*).

These properties were exploited to investigate the contribution of T-type calcium channels to the PF synaptic responses in PCs in slices of P15–P25 mice (see Methods). PCs were recorded in the whole-cell voltage clamp configuration, which ensures good steady-state control of the holding potential, preventing variability of the membrane potential and bistable behaviour, although it has little influence on rapid events in distal dendrites and spines (Roth & Häusser, 2001). The somatic clamp therefore does not prevent activation of rapid voltage-gated channels in distal compartments.

We stimulated PFs in coronal slices with a large-tipped (∼10–15 μm) extracellular electrode, aiming to deliver stable stimuli. As expected, the amplitudes of EPSCs evoked by GCL stimulation were smaller than those of EPSCs evoked by molecular layer (ML) stimulation: −90 ± 14 pA (n = 15) compared to −320 ± 45 pA (n = 10), respectively, when holding the PCs potential at –78 mV and using the same stimulus intensity range.

TTA-P2 was applied at 500 nM during repeated delivery of paired stimuli (see Methods). The onset of TTA-P2 EPSC inhibition (Fig. 2*D*) developed in less than 10 min. The EPSC amplitude was reduced by ∼20% for both GCL (P = 0.031; n = 9) and ML (P = 0.015; n = 11) stimulation (Fig. 2*E* and *F*). The time course of inhibition was similar to that observed when I_T was recorded in isolation in slices of very young mice. By contrast, EPSCs of $Ca_V3.1$ and $Ca_V3.3$ double KO mice evoked by ML stimulation did not show any sensitivity to TTA-P2 (Fig. 2*G* quantified in Fig. 3*B*) (McKay *et al.* 2006).

Surprisingly, the proportion of the EPSC that was blocked by TTA-P2 appeared to be independent of the EPSC amplitude, at least in the range tested. This is shown in Fig. 2*H*, which plots the fractional inhibition by TTA-P2 as a function of EPSC amplitude. The best fit line is flat (slope of $-2.10^{-4} \pm 2.10^{-4}$ pA^{-1}, P = 0.32; y-intercept = 0.26, P < 0.001; using a robust linear

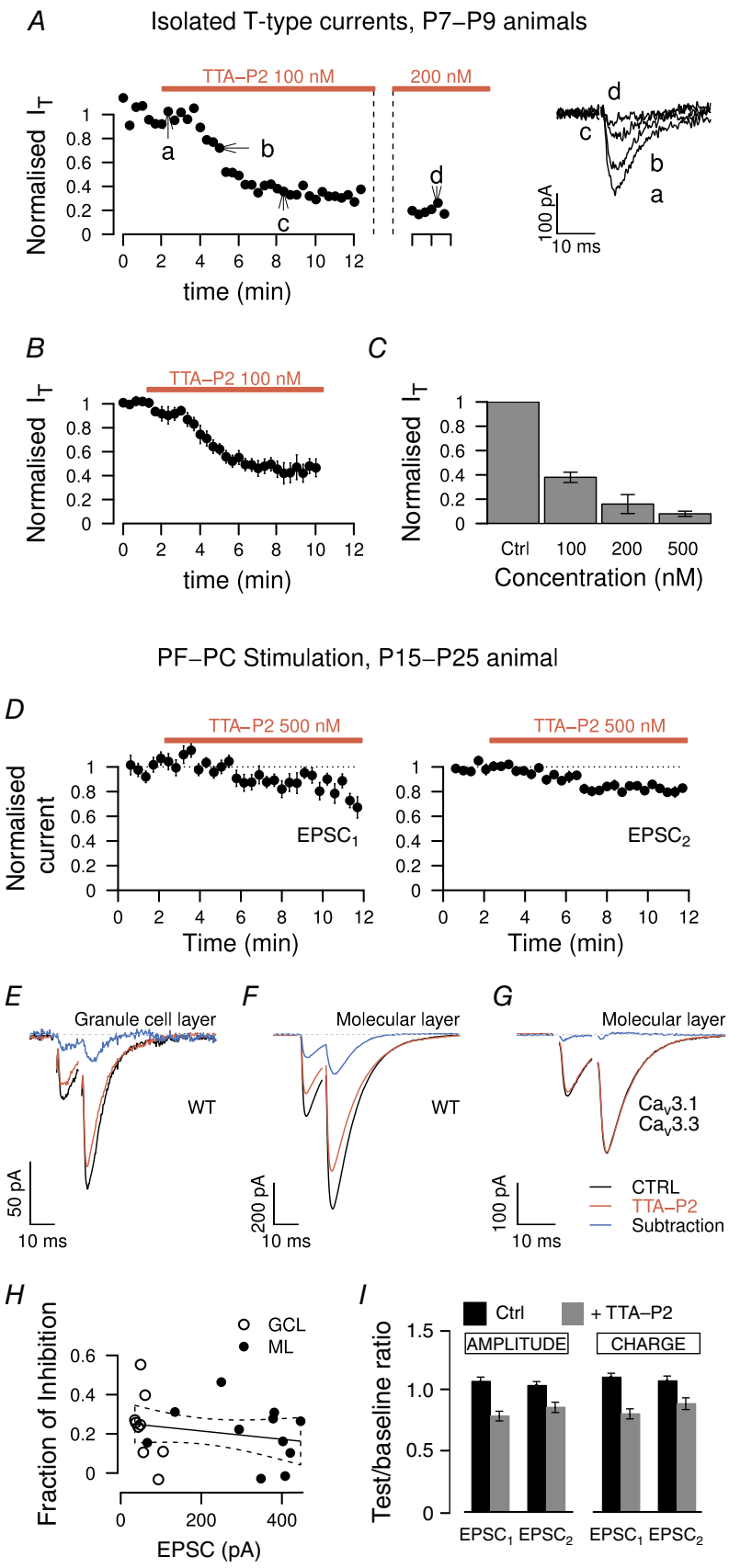

Figure 2. Inhibition of I_T and PF-PC EPSCs by TTA-P2
A–C, TTA-P2 inhibition of the isolated T-type current in P7-P9 mice (see Methods). *A*, left: example of TTA-P2 inhibition of normalized I_T. T-type currents were evoked by a step depolarization to –43 mV after prehyperpolarization to −83 mV for 500 ms. Right, T-type current traces at different times during the development of inhibition. *B*, mean normalized time course of I_T inhibition. I_T was inhibited to 40% by application of 100 nM TTA-P2. *C*, histogram showing the effect of increasing concentrations of TTA-P2, with full inhibition being attained near 500 nM. Calculated IC_{50} < 100 nM. *D–I*, TTA-P2 inhibition of evoked EPSCs in P15–P25 mice. *D*, paired EPSCs at a 10 ms interval were evoked every 8 s and their normalized amplitudes followed over time. The TTA-P2 effect is shown on $EPSC_1$ (left) and $EPSC_2$ (right). *E*, example of such paired EPSCs evoked by stimulation of the GCL (holding potential, −78 mV; the black and red traces represent mean EPSC traces before and after TTA-P2, respectively, and the blue trace shows the difference current). *F*, EPSCs obtained by stimulation in the ML. *G*, EPSCs obtained by ML stimulation in mice with a double deletion of the $Ca_V3.1$ and the $Ca_V3.3$ genes. *H*, fractional inhibition of PF-PC EPSCs evoked in the ML or GCL as a function of their control amplitudes. *I*, 600 nM TTA-P2 effect *vs.* explicit controls, starting from time zero, on the amplitude and charge of the EPSC. Histograms of test/baseline EPSC ratios, where the test condition was either control saline or application of TTA-P2.

fit, see Methods). Thus, although quite small sparse inputs were elicited with GCL stimulation, there was no indication of a threshold EPSC size for activation of T-type channels.

This was quite unexpected because T-type channels are highly voltage-dependent and larger EPSCs, especially with ML stimulation, would be expected to be associated with larger dendritic depolarizations. We suggest below that this behaviour might arise if T-type channels are only activated in spine heads subject to large depolarizations during synaptic activity.

Although our experimental protocols required a stable baseline for EPSC recordings and no marked changes of EPSC amplitudes over time were observed in the double KO mice (or when recording at more depolarized potentials; see below), we performed a series of recordings to compare the effect of TTA-P2 with respect to explicit control recordings of similar duration. For this purpose, 5 min after stabilization of the EPSC, the slices were superfused for a further 15 min with the normal saline solution or a solution containing 600 nM TTA-P2. Responses of ~300 pA were elicited by molecular layer stimulation and responses averaged over the 5 min baseline and between 10 and 15 min after drug application. As shown in Fig. 2*I*, a 20 ± 4.0% (mean ± SEM, $n = 11$) reduction of the baseline response by TTA-P2 was observed compared to an 8 ± 3.5% increase ($n = 11$) in the control recordings. The test–control difference was significant

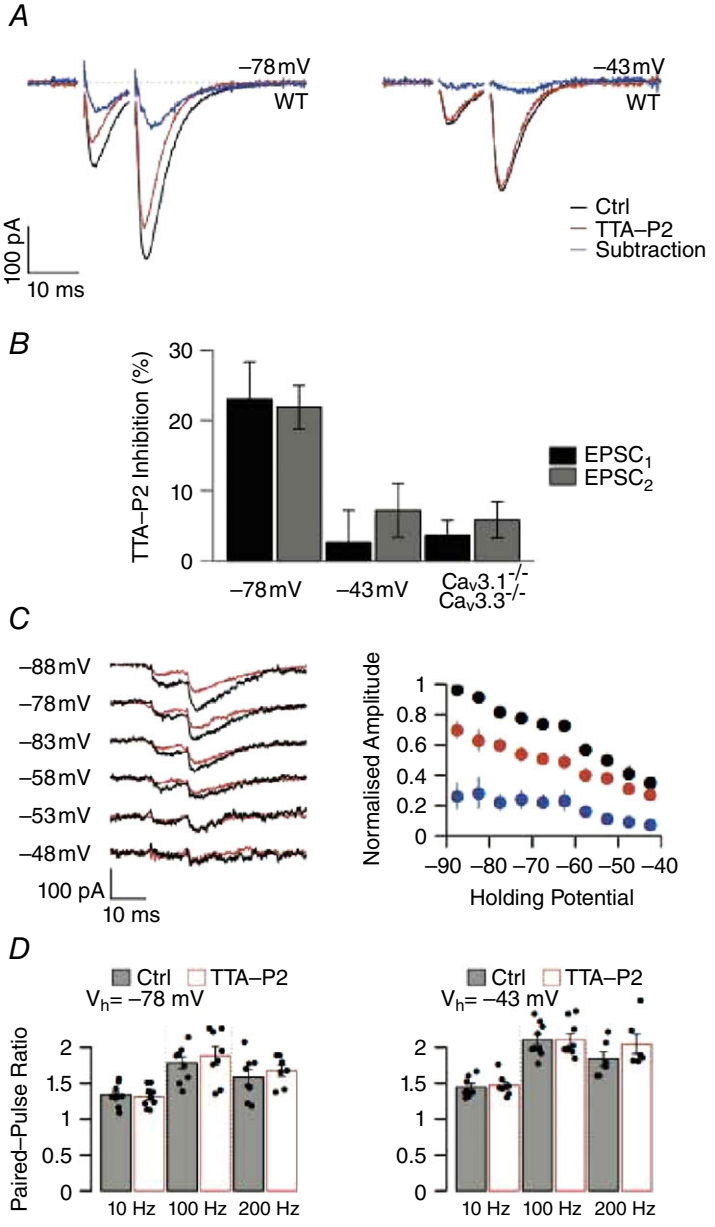

Figure 3. The TTA-P2 sensitive current is a postsynaptic voltage-dependent current
A, at −78 mV (left), TTA-P2 produces ~20% inhibition of paired EPSCs evoked at a 10 ms interval by GCL stimulation, whereas, at −43 mV (right), the effect of the inhibitor is much reduced. *B*, bar chart of the fraction of TTA-P2 inhibition at −78 mV and −43 mV on paired EPSCs (left and middle, respectively). Right, bars show TTA-P2 inhibition measured in the double KO ($Ca_V3.1^{-/-}$, $Ca_V3.3^{-/-}$) mice. *C*, left: the voltage sensitivity of the TTA-P2 current was evaluated by imposing different membrane potentials for 100 ms before stimulation. Black and red traces represent EPSCs recorded before and after drug perfusion. Right: *I–V* curve of PF-PC $EPSC_2$s before and after drug application (black and red markers, respectively). Blue symbols show the fraction of inhibition by TTA-P2. *D*, TTA-P2 did not change the PF-PC PPR (control conditions and in the presence of TTA-P2, grey and light grey bars, respectively) for any of the three tested frequencies (10, 100 or 200 Hz), at −78 mV or at −43 mV holding potentials (V_h); left and right bar plots, respectively.

($P = 8.5 \times 10^{-5}$). A similar reduction was seen in the charge: control 11% ± 3.2% increase *vs.* TTA-P2 19 ± 4.1% decrease ($P = 0.004$). We used alternating single and double pulses (10 ms interval) to obtain an accurate average of the second response by subtracting the average single-pulse response. This was used to evaluate the amplitude and charge of the second response, which both exhibited slightly smaller reductions with TTA-P2 than the first response. Amplitude: control 5 ± 3.2% increase *vs.* TTA-P2 15 ± 4.0% decrease ($P = 1.9 \times 10^{-5}$). Charge: control 8 ± 3.9% increase *vs.* TTA-P2 10 ± 4.8% decrease ($P = 0.005$). The T-type channel contribution to the EPSC can therefore amount to a quarter of the EPSC amplitude.

The mean rise (τ_{ON}) and decay (τ_{OFF}) time constants of the first EPSC at 10 Hz and at –78 mV were, respectively, 0.8 ± 0.3 ms and 7.5 ± 3.5 ms ($n = 6$) in control and 0.7 ± 0.2 ms and 9.2 ± 5.4 ms ($n = 6$) in TTA-P2 (all $P > 0.44$). TTA-P2 therefore had no obvious kinetic effect on the EPSC. One possible explanation is that both EPSC and the T-type calcium channel current are brief compared to dendritic filtering. We explore this by modelling below.

The synaptic recordings were performed with a 'physiological' solution, and so most voltage-gated channels were not blocked. However, in the subthreshold range relevant for small inputs, PCs behave linearly to a reasonable approximation, with the exception of Ih, which gates too slowly to be of relevance in the present study (Roth & Häusser 2001).

The effect of TTA-P2 is postsynaptic

The effect of TTA-P2 on synaptic responses could in principle arise through pre- and/or postsynaptic actions. At PF terminals, neurotransmitter release depends on presynaptic Ca^{2+} transients that are principally generated by P/Q-type and N-type, but also R-type calcium channels, whereas T-type channels are reported to be absent (Mintz *et al.* 1995; Brown *et al.* 2004; Myoga & Regehr 2011). We nevertheless aimed to confirm that the effect of TTAP-P2 was postsynaptic. We set the PC holding potential at –43 mV to inactivate completely postsynaptic T-type calcium channels. At this potential, TTA-P2 did not significantly inhibit the EPSC: 2.7 ± 4.5%, (mean ± SEM, $n = 7$, $P = 0.58$; values are for EPSC1) compared to 23 ± 5.3% ($n = 7$) at −78 mV, (Fig. 3*A* and *B*). A similarly small effect of TTA-P2 was observed in slices from $Ca_V3.1$ and $Ca_V3.3$ double KO mice: 3.7 ± 2.1% ($n = 5$). The inhibition by TTA-P2 was significantly stronger at –70 mV than at –43 mV or in the double KO ($P = 0.014$ and $P = 0.0043$, respectively; Wilcoxon rank sum test).

We characterized the voltage-dependence (Fig. 3*C*) of the TTA-P2-sensitive current (blue traces in Fig. 3*A*). The current–voltage relationships of the EPSC and TTA-P2 sensitive current were studied using 100 Hz paired-pulse stimulation at potentials varying from −88 mV to –43 mV in steps of 5 mV ($n = 6$) (Fig. 3*C*). Above –40 mV, we could not ensure good voltage clamp as a result of potassium channel activation. A TTA-P2-sensitive component could only be evoked at holding potentials ranging from –88 mV to −50 mV, corresponding to the range encompassed by the inactivation curve as we will see below. All of the above characteristics indicate that a postsynaptic T-type component is activated by the EPSC-induced depolarization.

We also monitored the PPR, which indirectly reflects release probability and Ca^{2+} levels in the presynaptic endings, before and after TTA-P2 application (Fig. 3*D*). At –78 mV, application of the drug did not change the PPR significantly ($P > 0.15$ for all frequencies) (Table 1).

These results suggest that TTA-P2 does not affect transmitter release and point to an exclusively post-synaptic origin of the TTA-P2-sensitive component.

EPSC inhibition by TTA-P2 is constant for different paired pulses intervals

We characterized the effect of stimulation frequency on the TTA-P2-sensitive EPSC component (Fig. 4). We applied paired stimuli at intervals of 100, 10 and 5 ms in the ML. The degree of inhibition by TTA-P2 was similar for the first and second EPSCs ($EPSC_1$ and $EPSC_2$; Fig. 4*A* and *C*). As shown in the histogram of Fig 4*B*, the effect of TTA-P2 on $EPSC_1$ and $EPSC_2$ was very similar at all frequencies.

T-type calcium channels display voltage-dependent inactivation. One might therefore expect the post-synaptic T-type channels to become inactivated during an EPSC and consequently contribute a reduced current to succeeding responses. It was therefore surprising to observe that TTA-P2 had little effect on PPR, suggesting that inactivation was not significant. We argue below that brief depolarization will favour deactivation instead of inactivation of T-type channels, enabling their repetitive activation. However, modelling below will also suggest a more complex mechanism in which the T-type calcium current in spines is recruited at different times in the train of stimuli depending on the strength of the individual synapses.

The above experiments were carried out in voltage clamp mode. It might be expected that this recording configuration would limit the activation of voltage-dependent channels, although, in reality, the somatic clamp would probably have little influence on rapid dendritic events. To clarify this issue, we examined the contribution of T-type channels to synaptic transmission under more physiological conditions. Using the

Table 1. Absence of TTA-P2 effect on PPR at different frequencies

		10 Hz	100 Hz	200 Hz
−78 mV	Control	1.34 ± 0.04 (10)	2.22 ± 0.08 (10)	2.45 ± 0.11 (8)
	TTA-P2	1.31 ± 0.04 (10)	2.4 ± 0.1 (10)	2.5 ± 0.1 (7)
−43 mV	Control	1.42 ± 0.05 (8)	2.54 ± 0.11 (8)	2.5 ± 0.1 (6)
	TTA-P2	1.45 ± 0.05 (8)	2.44 ± 0.06 (9)	2.7 ± 0.1 (6)

Data are the mean ± SEM (*n*).

same $KMeSO_4$ pipette recording solution but working in current clamp, we held the PC at around –72 ± 6 mV (mean ± SD, $n = 19$) to deinactivate the calcium channels, and also to prevent firing and bistable behaviour. TTA-P2 application induced a reduction of the EPSP amplitude (Fig. 5*A–C*) with a time course similar to that observed in the experiments above (compare Fig. 5*B* with Fig. 2*A* and *G*). On average, inhibition amounted to 15% (Fig. 5*C* and Table 2). The different holding potentials in the voltage and current clamp experiments (–78 mV and –72 mV, respectively) would be expected to reduce T-type channel activation in the current clamp experiments. As with EPSCs, the degree of EPSP inhibition by TTA-P2 did not depend on the stimulation intensity (Spearman correlation test: $P = 0.6$, pooling values from ML and GCL stimulations) or on the stimulation position: inhibition for GCL stimulation, 13 ± 3%; inhibition for ML stimulation 17 ± 3% ($P > 0.33$) (Fig. 5*E*).

Block of T-type calcium channels did, however, induce a slight hyperpolarization of the membrane potential (3 ± 1%, $n = 9$, $P < 0.01$), which may relate to the existence of a small window current at potentials around −70 mV (see biophysical characterization below).

TTA-P2 had no significant effect on the mean EPSP decay time or the subsequent after-hyperpolarization (AHP) (Fig. 5*D* and *F*). The weighted decay time constant estimated by a double exponential fit, the 80–20% decay time, and the AHP amplitude after TTA-P2 application are shown in Table 2.

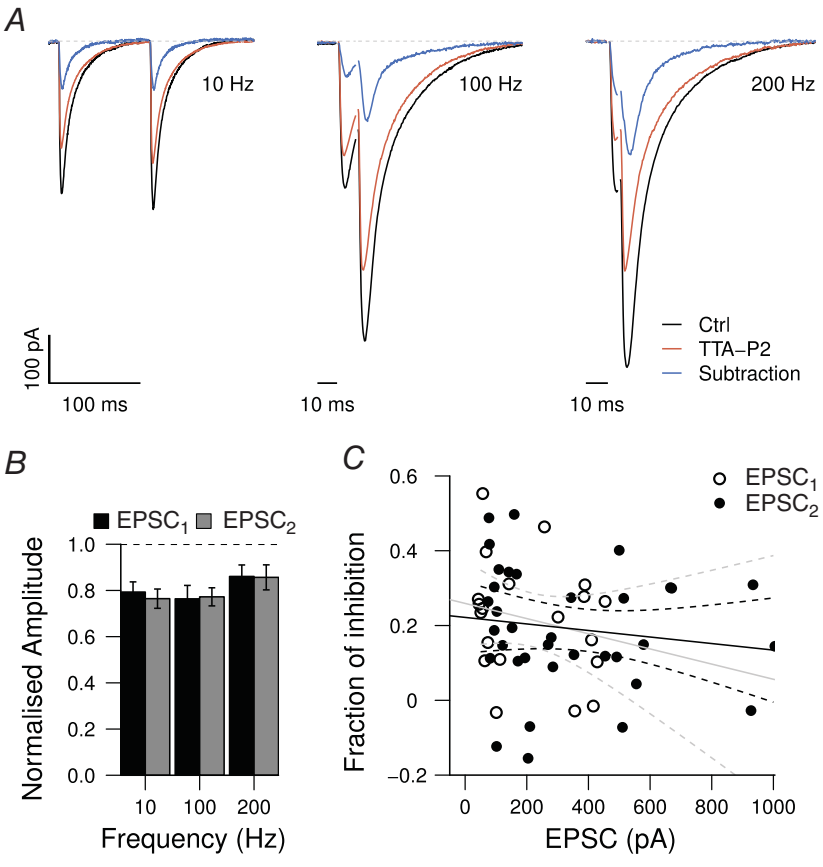

Figure 4. Absence of frequency-dependence of the inhibition by TTA-P2
A, EPSCs elicited by ML stimulation at 10, 100 or 200 Hz, showing inhibition by TTA-P2. *B*, corresponding histograms showing the reduction in the amplitude of $EPSC_1$ and $EPSC_2$ at 10, 100 and 200 Hz. *C*, linear relationship between the fraction of inhibition and the amplitude of EPSC1s and EPSC2s for all three frequencies (grey and black, respectively; $n = 20$; continuous and dotted lines show regression and ± 95% confidence interval, respectively).

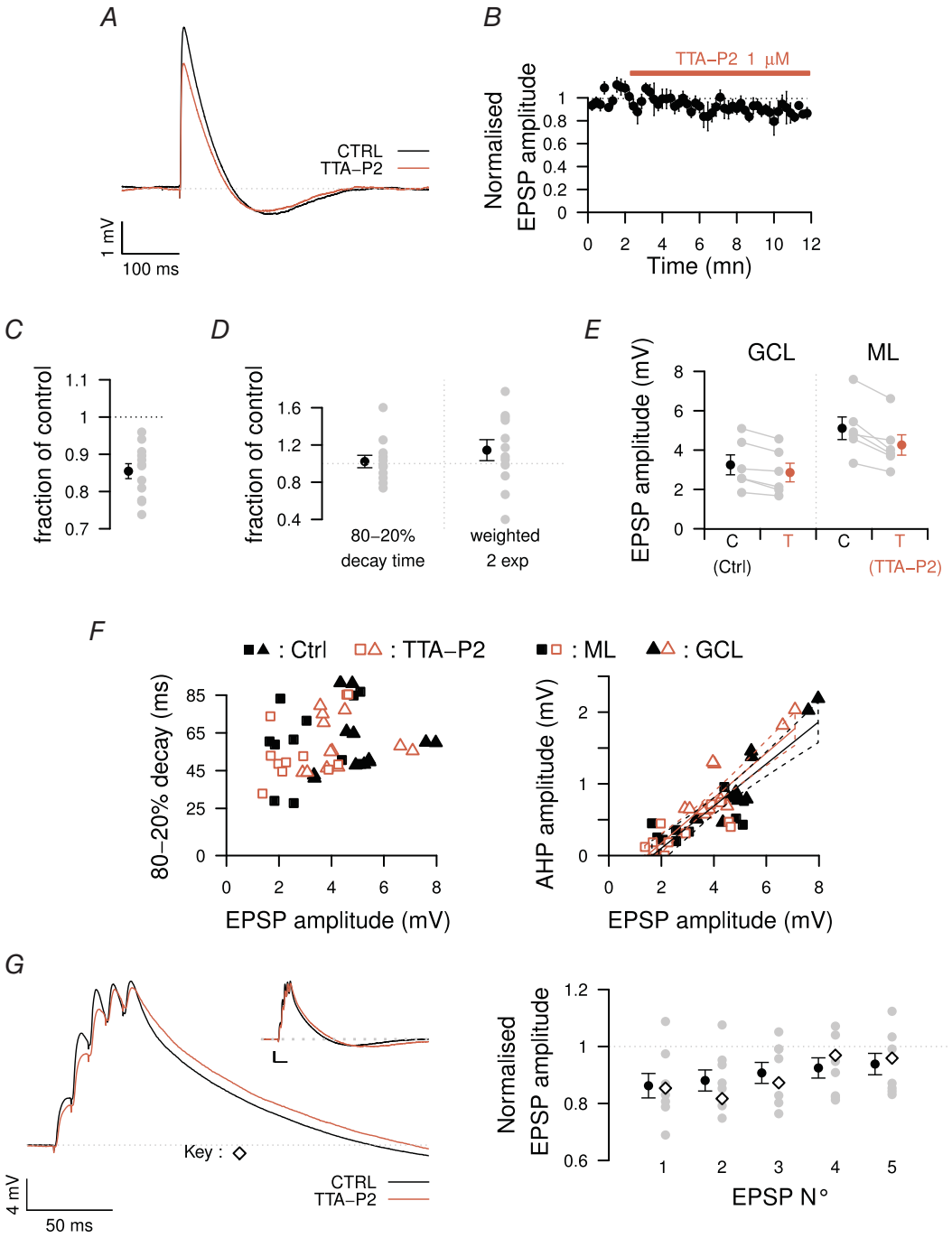

Figure 5. Inhibition of PF-PC EPSPs by TTA-P2
A, typical EPSP traces showing the reduction of amplitude between control and in the presence of 1 μM TTA-P2 (black and red traces, respectively). *B*, mean time course of the inhibitory effect of TTA-P2 on the normalized EPSP amplitude. *C–D*, effects of TTA-P2 on EPSP amplitude (*C*) and decay time (*D*). Data from ML and GCL stimulation are pooled in (*B*) to (*D*). *E*, effect of TTA-P2 on EPSPs elicited by GCL and ML stimulation. *F*, 80–20% decay time (left) and AHP amplitude (right) *vs.* EPSP amplitude. Control and TTA-P2 values, filled black and empty red symbols, respectively; ML and GCL stimulation, square and triangle symbols, respectively. Regression lines are shown in black and red for data points before and after the addition of TTA-P2, respectively (95% confidence interval in dashed lines). *G*, left: typical trace before and after TTA-P2 stimulation during a train of five GCL stimuli at 100 Hz. Averaged traces. Inset: same traces at a different scale highlighting the AHP (scale bars = 50 ms and 4 mV, respectively). Right: graph showing the normalized EPSP peak amplitudes at each stimulus. The diamond symbol represents the example on the left. Data are the mean ± SEM.

Table 2. TTA-P2 effect on a single EPS

	EPSP amplitude	Weighted time constant	Decay time (80–20%)	AHP amplitude
Fraction of control after TTA-P2	0.85 ± 0.02	1.14 ± 0.11	1.02 ± 0.31	0.86 ± 0.25

Data are the mean ± SEM % ($n = 12$); all $P > 0.20$, except for the EPSP amplitude ($P = 0.0005$).

Because granule cells are able to emit short bursts of action potentials at very high frequencies (Chadderton *et al.* 2004; Jorntell & Ekerot, 2006), we measured the effect of TTA-P2 on EPSP trains at different frequencies. Interestingly, as in the voltage clamp experiments, TTA-P2 inhibited similar fractions of the first and second responses in a paired-pulse protocol, independently of the interval. Thus, compared to the 15% inhibition of the first response, the second was reduced by 17 ± 2% at 1 Hz ($n = 10$, $P < 0.01$), 11 ± 3% ($n = 9$, $P < 0.05$) at 100 Hz and 17 ± 4% ($n = 4$, $P < 0.05$) at 200 Hz. We also examined the effect of TTA-P2 on responses to a train of five stimuli at 100 Hz. During a burst, TTA-P2 induced a roughly constant fractional inhibition over the first three EPSPs, with a lesser effect occurring during the last two (Fig. 5*G*), presumably because of inactivation during the maintained depolarization. The EPSP amplitudes during trains applied in the presence of TTA-P2, normalized to the corresponding amplitudes under control conditions, were, respectively: $EPSP_1$, 86 ± 4% ($P < 0.05$); $EPSP_2$, 88 ± 4% ($P < 0.05$); $EPSP_3$, 91 ± 4% ($P < 0.05$); $EPSP_4$, 93 ± 4% ($P = 0.07$); and $EPSP_5$, 94 ± 4% ($P = 0.14$) ($n = 8$) (Fig. 5*G*). The decay did not change: the weighted time constant from a bi-exponential fit was 95 ± 11% of control ($n = 8$, $P = 0.74$); 80–20% decay time, 98 ± 6% ($n = 8$, $P = 0.95$). There was a slight and non-significant diminution of the AHP amplitude: 83 ± 9% of control ($n = 8$, $P = 0.078$). The contribution of the T-type channel-dependent component was therefore substantial for the first three EPSPs at stimulation intervals occurring physiologically.

T-type calcium channel activation during simulated dendritic EPSP waveforms

Although somatic recordings report the charge arising from channel activation, they give little insight into the precise kinetics and voltage-dependence of I_T recruitment in dendrites and spines. To investigate the possible range of behaviours of native channels, we made use of the fact that PCs in very young animals (7–9 days) can be adequately voltage clamped (for isolation of I_T, see Methods). In this preparation, we examined I_T recruitment in response to simulated EPSP waveforms (sEPSP) with a range of kinetics. I_T was isolated by subtraction using TTA-P2. Figure 6*A* illustrates I_T evoked by fast sEPSPs, the amplitude of which was varied from 15 to 50 mV. As expected, Ca_V3 recruitment increased with depolarization. It was striking, however, that significant activation required depolarizing steps of ∼20 mV.

We also analysed how the sEPSP kinetics affected I_T activation by using four waveforms with distinct kinetics (τ_{ON} = 1–5 ms; τ_{OFF} = 5–100 ms; see colour code in Fig. 6*D*); those with faster time courses were intended to mimic signals that probably arise in distal dendritic elements, whereas the more filtered waveforms correspond to those occurring in the soma or proximal dendrites (Fig. 6*B*). Strikingly, the I_T waveforms recorded during the sEPSPs displayed quite similar time courses to the sEPSP, whatever the sEPSP shape considered. Traces in Fig. 6*B* (right) illustrate the I_T evoked by 5 mV sEPSPs from a holding potential of −63 mV after a 250 ms hyperpolarization to –83 mV. I_T rise time varied with that of the sEPSP, whereas the I_T decay phase followed the sEPSP decay until limited by inactivation (Fig. 6*B* and *C*). Thus, for slower waveforms, the maximal I_T decay constant was 9.8 ± 1.2 ms ($n = 10$), a value quite similar to the inactivation time constant (Fig. 7*B*). From a holding potential of −73 mV (without a prehyperpolarization), we obtained similar results (Fig. 6*B*, left). These results show that T-type calcium channels in PC dendrites activate sufficiently quickly to follow rapid depolarizing events lasting a few milliseconds.

Bursting activity and activation of I_T

We also exploited the well clamped immature PCs and sEPSPs to investigate I_T recruitment during repetitive synaptic activity. In designing the sEPSPs, we implemented realistic paired-pulse facilitation for the following frequencies: 10, 50, 100 and 200 Hz (see Methods). The frequency was critical in the summation of successive sEPSPs. At low frequency, the individual sEPSPs were essentially discrete events. By contrast, at high frequency (200 Hz), the successive sEPSPs formed a single large depolarization and, similarly, the recruitment of I_T followed the time course of the burst of sEPSPs (Fig. 6*E*, left). We compared the steady-state T-type current activation curve with the voltage dependence of I_T activation during the bursts of sEPSPs at a frequency of 200 Hz in the same cell. The activation curve during sEPSPs was slightly right-shifted with respect to the

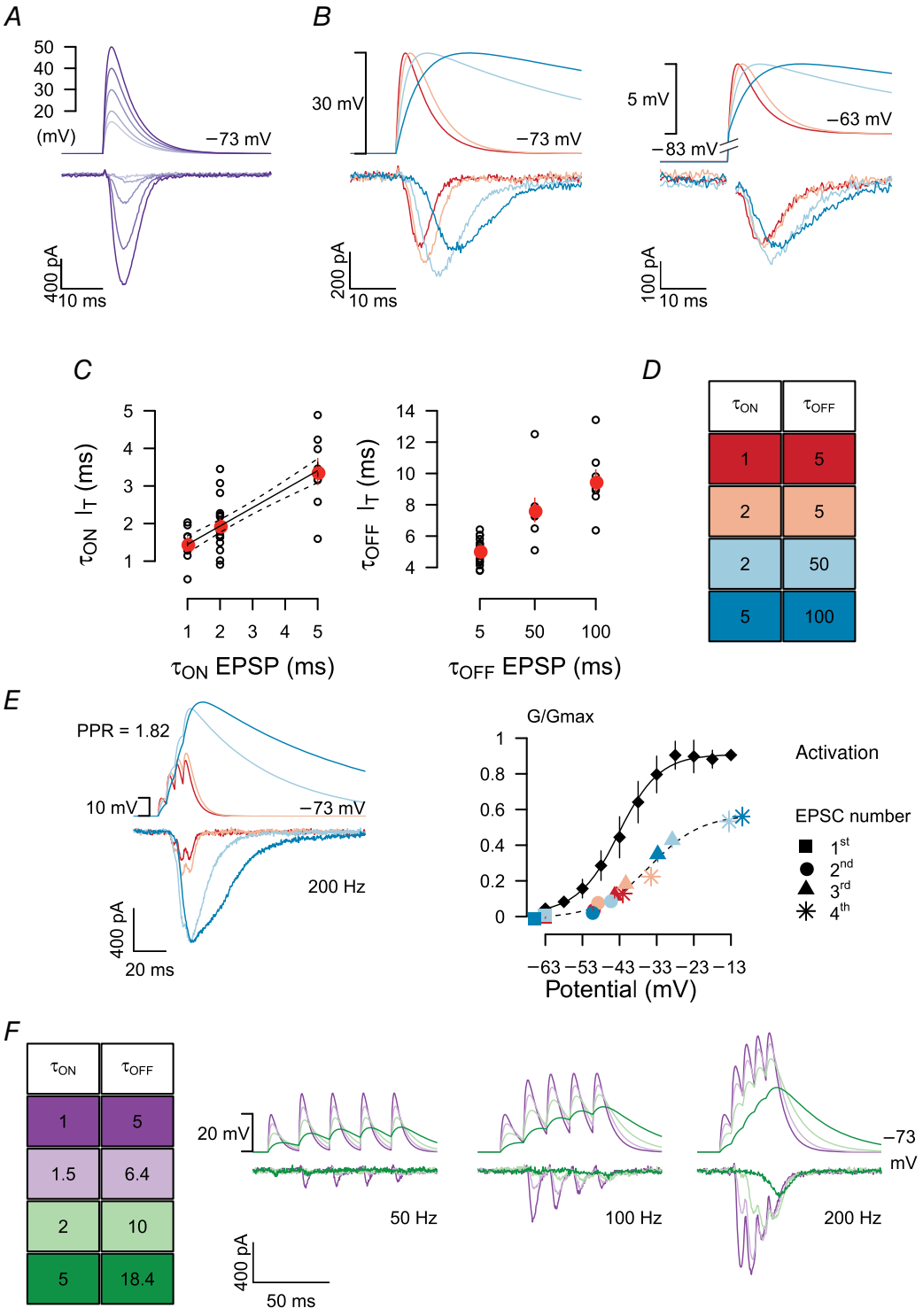

Figure 6. Characteristics of I_T evoked by EPSP waveforms
A–D, I_T kinetics during a single simulated EPSP generated by two exponentials according to the colour code given in (*D*). *A*, effect of amplitude. Simulated EPSPs were generated using two exponentials, with time constants τ_{ON} and τ_{OFF} of 2 and 5 ms. Larger EPSPs yield I_T values with faster rise times and shorter delays. *B*, effect of changes in time course. Left: EPSP waveforms (upper traces) were imposed from −73 mV; lower traces show the corresponding I_T. Right: smaller EPSP waveforms with the same kinetics imposed from a holding potential of −63 mV preceded by a 250 ms pre-hyperpolarization to −83 mV. *C*, linearity between τ_{ON} (left) or τ_{OFF} (right)

steady-state curve ($V_{1/2} = -35$ mV, compared to -47 mV) and had an attenuated slope, presumably resulting from cumulative inactivation (Fig. 6*E*, right). Note that I_T was only evoked at the second sEPSP; the first sEPSP was insufficient to activate T channels significantly (Fig. 6*E*).

We performed similar experiments for a range of waveforms simulating bursts of five sEPSPs. sEPSPs of smaller amplitude and slower decay caused the threshold potential for T-type activation to be reached only after a delay and in the presence of ongoing inactivation (Fig. 6*F*). Only if the sEPSP amplitudes were sufficiently large could a significant activation of T-type channels be observed at lower frequencies, whereas rapid kinetics preserved T-type channels from inactivation, presumably because the channels deactivated, rather than inactivated, following the rapid repolarization (Fig. 6*F*). In these experiments, I_T would typically decrease after the third sEPSP, as expected from the current clamp recordings of EPSPs. At 200 Hz, the decay time constants of the I_T values elicited by the last sEPSP were: 7.7 ± 0.6, 7.7 ± 0.1, 8.0 ± 0.9 and 9.0 ± 1.1 ms for sEPSPs τ_{OFF} of 5, 6.4, 10 and 18.4 ms, respectively ($n = 8$). These results show that T-type channels undergo only mild inactivation during high frequency synaptic activity with rapid kinetics.

T-type calcium channel biophysical properties

T-type channels are often considered to be slowly activating and rapidly inactivating (Burgess *et al.* 2002), whereas the results above highlight the relative rapidity of activation and deactivation. We therefore performed a biophysical characterization of the T-type current in young PCs (7–9 days old) at 32°C. The kinetic parameters that we measured are reported in Fig. 7. Activation and deactivation occur with time constants ranging from 0.5 to 2.5 ms ($n = 16$) (Fig. 7*A*), whereas inactivation above -53 mV develops in less than 7 ms ($n = 16$) (Fig. 7*B*, inset). These fast kinetics are very similar to the I_T time course measured in an heterologous system containing $Ca_v3.1$ subunits (Iftinca *et al.* 2006), supporting the notion that a majority of Purkinje T-type calcium channels are composed of the $Ca_v3.1$ subunit. Assuming that activation and deactivation are opposite processes, their voltage-dependences are controlled by factors of α and 1-α, respectively, where α relates to the position of the voltage sensor in the membrane. Accordingly, the deactivation and activation time constants τ_m at the successive potentials could be described by the inverse of the sum of two Boltzmann equations (see Appendix), yielding a maximum at –48 mV (Fig. 7*A*), in good agreement with the experimentally determined potential of half-activation: -45 ± 1 mV ($n = 29$), (Fig. 7*D*, filled symbols and Fig. 7*C*, upper traces). We used the same formalism for inactivation and recovery processes; a similar fit (Fig. 7*B*) yielded a maximal time constant at –83 mV, in good agreement with the -78 ± 1 mV ($n = 12$) potential of half-inactivation estimated from the steady-state inactivation curve (Fig. 7*C*, lower traces and 7*D*, open symbols). We further showed that the parameters of half-inactivation and half-activation were conserved in the presence of 100 nM TTA-P2 (data not shown), indicating that the blocking effect of TTA-P2 does not involve an alteration of Ca_V3 gating properties.

Although we blocked most voltage-gated conductances other than calcium channels, some voltage escape could nevertheless have occurred, which would facilitate activation of T-type channels. The main conclusion that we draw below is that synaptic inputs recruit these channels more easily than expected on the basis of the above characterization. The presence of significant voltage escape here would only exacerbate this difference.

These experiments demonstrate that T-type calcium current kinetics are sufficiently rapid at 32°C to follow even fast EPSPs.

Modelling I_T recruitment in spines and dendrites

Figure 2*H* showed that small EPSCs (~50 pA) elicited by granule layer stimulation displayed a level of inhibition by TTA-P2 similar to that of large EPSCs (400 pA) elicited by molecular layer stimulation. A large EPSC elicited by ML stimulation would be expected to produce a much

of the EPSP waveform (pre-hyperpolarization protocol as in *B* right) and of the corresponding I_T. Continuous and dashed lines show linear regression ± 95% confidence intervals. *D*, colour code for the four waveforms simulating EPSPs that were generated by two exponentials with τ_{ON} and τ_{OFF} as indicated (ms). *E–F*, I_T activation during burst activity. *E*, left: traces illustrate T-type channel recruitment during a four stimulus burst at 200 Hz. The second and subsequent stimuli were 1.82-fold larger than the first EPSP, to account for paired-pulse facilitation, as illustrated by the command waveforms (upper traces); same colour code as in (*D*). The corresponding I_T is shown in traces below. Right: normalized activation curve (black diamonds) and during I_T elicited by 200 Hz bursts of four simulated EPSPs (coloured symbols). Maximal I_T conductance induced by the four stimuli was normalized to the maximal activation reached in the same cell, then plotted against the membrane potential reached at the corresponding stimulus number. *F*, I_T evoked by command waveforms mimicking different dendritic filtering effects. Rise times for the four waveforms were 1, 1.5, 2 and 5 ms with decreasing amplitude; colour code at left. Bottom traces show activation of I_T during five stimuli at 50 Hz (left), 100 Hz (middle) and 200 Hz (right). The second and the subsequent stimulus amplitudes were increased by the PPR for each frequency (1.53, 1.75, and 1.82 for 50, 100 and 200 Hz, respectively).

larger and concentrated dendritic depolarization. It was therefore surprising that the strongly voltage-dependent T-type calcium channel current did not contribute a larger fraction of charge than during a weak, dispersed EPSC following GCL stimulation. One possible explanation is that spines are subject to stronger depolarizations than dendrites and that T-type channels are mostly recruited in spines. Because it remains difficult to measure spine calcium or voltage responses during sparse synaptic stimulation (as opposed to the use of compact PF bundles recruited with molecular layer stimulation), we examined this hypothesis by modelling propagation of a unitary EPSP from the spine to soma and the recruitment of T-type channels with the kinetic properties determined above (see Methods). We assumed for this modelling that all of the TTA-P2-dependent current is carried by T-type calcium channels.

A key parameter in the model is the spine neck resistance because this governs the strength of the spine depolarization with respect to the dendritic potential. There has been only one, preliminary, measurement of this parameter in PCs: Häusser *et al.* (1997) found a value of 44 MΩ (Häusser M, Parésys G and Denk W. Society for Neuroscience; abstract cited in Roth & Häusser, 2001). However, using this value with a plausible synaptic conductance (see below), very little activation of I_T occurred, in apparent contradiction to the recruitment observed with small EPSPs (Figs 2*H* and 5*E*) elicited by GCL stimulation (Fig. 2*H*). To attain the depolarization of 20 mV necessary to activate T-type channels in spines (Fig. 6*A*), we were obliged to increase the spine neck resistance to almost 1 GΩ (Segev & Rall 1988). There are, however, reports of high-resistance spine necks in other cell types (Bloodgood & Sabatini 2005; Araya *et al.*

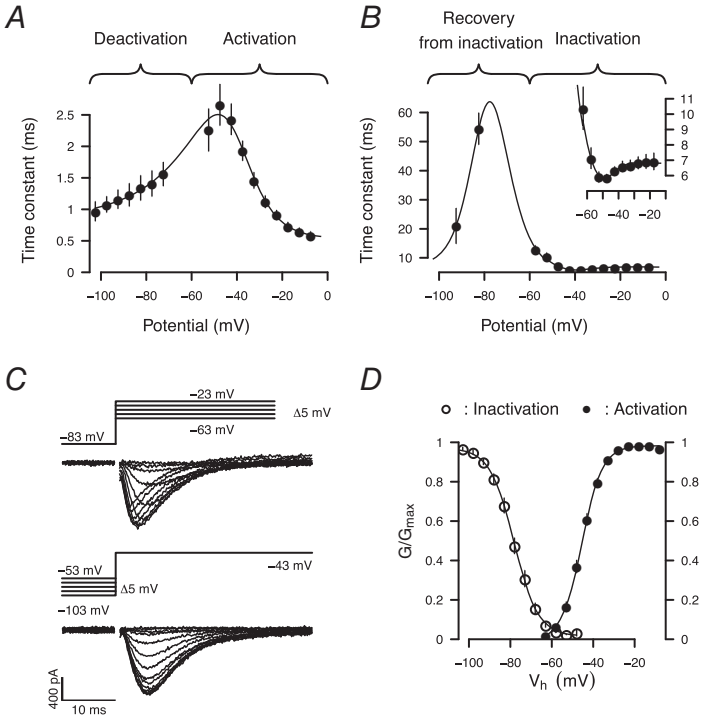

Figure 7. Biophysical properties of native T-type calcium channels at 32°C
A, measured activation and deactivation time constants as a function of membrane potential. *B*, measured time constants for inactivation and recovery from inactivation as a function of membrane potential. Inset: at more depolarized potentials, inactivation time constants display a 'rebound' typical of T-type calcium channels. Activation and inactivation time constants (τ_m and τ_h, respectively) were fitted (continuous line in each graph) using a Hodgkin–Huxley formalism (see Methods). I_T time course (activation and inactivation time constants) was characterized by a Hodgkin–Huxley fit of I_T obtained as in the upper traces in (*C*) at the indicated potentials. The deactivation time constant was measured by fitting with one or two exponentials the decaying current during the repolarization to the indicated potential after a depolarization to −43 mV. The time constant for recovery from inactivation was estimated by following the current amplitude at the last step of the following protocol: after a 10 s inactivation, T-type channels were deinactivated for variable times by a pre-hyperpolarization, and then activated by a depolarization to −43 mV. *C*, current traces obtained from activation and inactivation protocols (upper and bottom traces, respectively). Activation protocol: after a prehyperpolarization to −83 mV, I_T was elicited by step depolarizations with 5 mV increments from −63 mV to −8 mV. Inactivation protocol: after step hyperpolarizations with 5 mV increments from −103 mV to −63 mV, I_T was elicited by depolarization to −43 mV. *D*, I_T activation and inactivation curves.

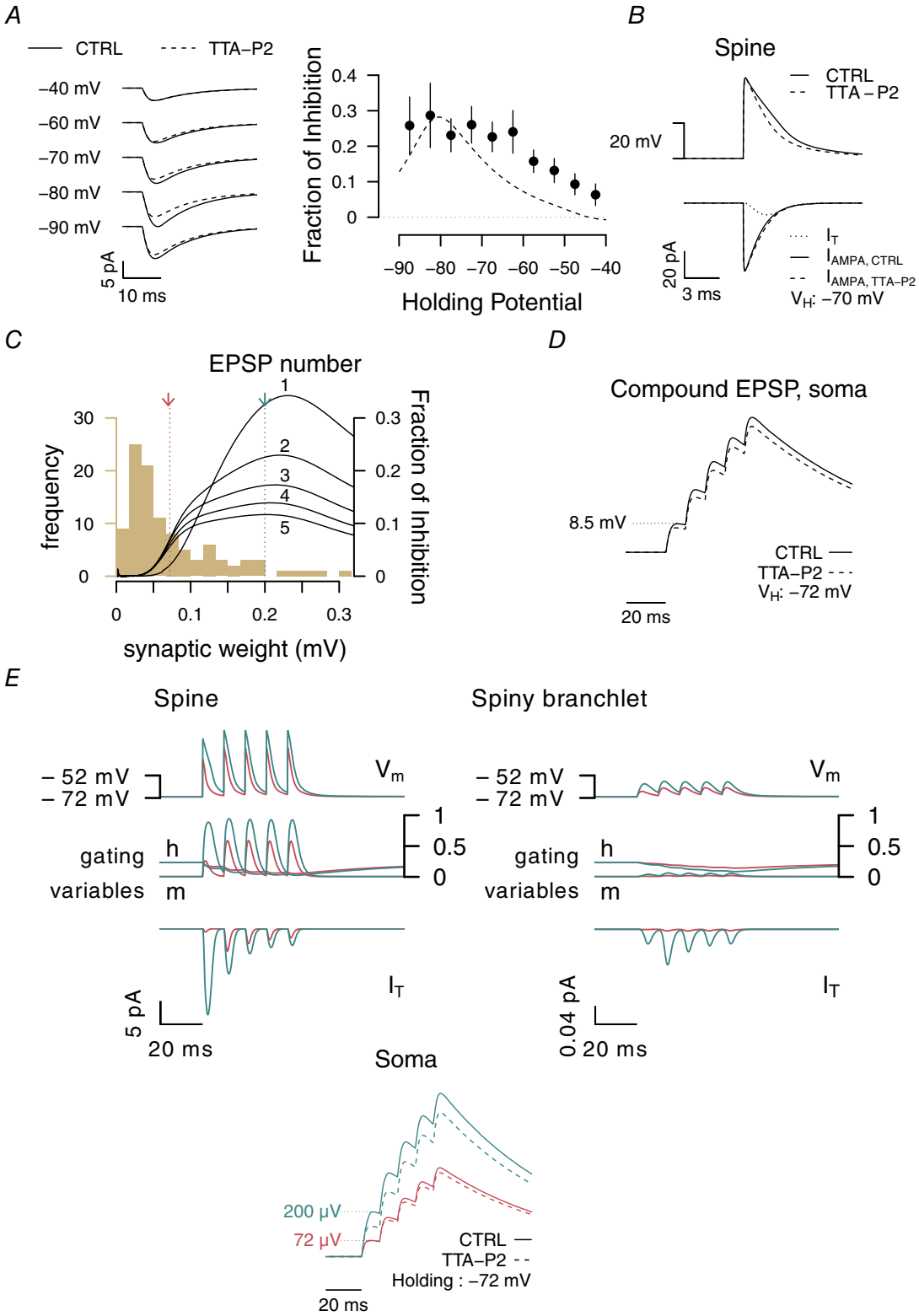

Figure 8. Model of spine and dendrite I_T
A–C, simulations for a synaptic input of 2.5 nS *A*, left: simulated EPSC from one spine recorded at the soma at different holding potentials before (CTRL) and after I_T removal from the model (TTA-P2). Right: experimental (Fig. 3*C*) and simulated fractional inhibition of the EPSC-voltage relation; black dots and dashed line, respectively. *B*, top: EPSP at the spine. Bottom: I_T and AMPA current at the spine. *C*, PF-PC synaptic weights histogram in brown (left ordinate, from paired-recordings; Brunel *et al.* 2004) and fraction of inhibition by TTA-P2 of the amplitudes of five

2006; Grunditz *et al.* 2008). With this parameter value, we were able to reproduce the experimentally observed I_T proportion and voltage-dependence, for an isolated (sparse) synaptic input (Fig. 8*A* and *B*).

There is strong evidence that PF-PC synapses can have widely varying strengths (or weights). Recordings of unitary GC-PC synaptic responses in adult rat have shown a skewed distribution of weights (Brunel *et al.* 2004; the histogram is reproduced in Fig. 8*C*), with a mean of ∼70 μV (equivalent to an EPSC of 8 pA; Isope & Barbour, 2002). Immunochemical studies of synaptic AMPA receptor numbers (Masugi-Tokita *et al.* 2007) suggest that their wide variation pobably explains much of the electrophysiological variation. In a spine with a high spine neck resistance, the activation of spine T-type channels could depend strongly on the AMPA synaptic conductance.

We examined this in a simplified model incorporating an active spine in a dendritic branch (see Methods). The strengths of the synaptic inputs were based upon the recordings of unitary granule cells-PC connections *sensu* Isope & Barbour (2002) who established the approximate conservation of synaptic charge under their experimental conditions. Knowing the synaptic charge of a connection supplies a contraint linking the synaptic current time constant and its amplitude (assuming a single-exponential decay): charge = amplitude × τ. The modelling shown below respects this constraint.

The recruitment of T-type calcium channels in spines with a high neck resistance and receiving a relatively strong input is shown by the curves superimposed on the weights histogram in Fig. 8*C*. Each curve plots the fraction of the somatic EPSP that is caused by T-type channel activation as a function of synaptic weight (somatic EPSP amplitude). The different curves represent the fractional T-channel contribution at the first to fifth EPSP peaks during a simulated train of inputs at 100 Hz. The key point to note is that weaker synapses are unable to activate significant I_T. However, because these synapses display paired-pulse facilitation, there is a subpopulation of synapses where the second and subsequent responses will be facilitated above the threshold for activating I_T. This can be seen in the leftward shift of curves for the second and subsequent EPSPs. Synapses with a weight of 70 μV (Fig. 8*C*, red arrow) would display this behaviour.

Because of this possible variation of synaptic behaviour, we generated a compound EPSP by summing unitary EPSPs independently in the model according to the frequency of each synaptic amplitude (Fig. 8*D*). We then used this compound response to set the T-type channel conductance in the spine (2 nS), aiming to recover the 15% I_T contribution to EPSPs at −72 mV. Finally, the rate at which the I_T contribution to the EPSP waveform declined during the train of responses turned out to be sensitive to the decay time constant of the synaptic conductance. This is because fast synaptic responses cause channels to deactivate rather than to inactivate. We found that a time constant of 1 ms allowed us to recover the observed slow decline of the I_T contribution to successive EPSPs, a value close to the 1.3 ms reported by Barbour *et al.* (1994) and Häusser & Roth (1997) (but at room temperature) in PCs.

This set of parameters, which enabled reproduction of the experimental observations, was used in the model shown in Fig. 8. Detailed simulations of spine, dendritic and somatic behaviour for two different strength unitary synaptic inputs are shown in Fig. 8*E*. The size of the smaller input (red arrow, Fig. 8*C*) was chosen to highlight the recruitment of an I_T by paired-pulse facilitation, whereas the other input (Fig. 8*C*, green arrow) was sufficient to activate the T-type channels during the first synaptic response. The simulations plot the membrane voltage in the different compartments and the gating parameters of the T-type channels. We see that the dendritic depolarization is too small to activate the T-type channels, whereas the stronger depolarization in the spine is able to do so. The different strength synapses also differ in the speed with which T-type channels inactivate, a process that can be observed during simulated trains of responses. Inactivation proceeds more rapidly at stronger synapses. We also verified that synaptic input in other dendrites (i.e. the large dendritic compartment in our model) would not contribute significantly to the individualized dendrite. Thus, activating a 20 nS peak conductance in the large compartment only depolarized the individualized dendrite by 300 μV. At least in our model in a sparse activity regime, a quite concentrated input to a single or neighbouring dendrites would be required for the dendritic depolarization to activate T-type channels directly.

In summary, this model of the T-channel contribution to sparse synaptic input is able to reproduce all of our experimental findings but requires a high spine neck resistance to do so. Under these conditions, the observed I_T arises almost exclusively in active spines,

somatic EPSPs at 100 Hz (right ordinate, continuous lines). Red and green arrows represent two particular synaptic weights illustrated in (*E*). *D*, compound EPSP at the soma generated by summing simulated unitary EPSPs according to the frequency of each synaptic weight. The fraction of inhibition by TTA-P2 of the five EPSPs amounted to 15%, 12%, 10%, 8% and 7%. *E*, simulated EPSPs at 100 Hz for two synaptic weights (green and red, see arrows in *C*) in the spine, spiny branchlet and somatic compartment. V_m, m, h and I_T are the local potential, T-type gating variables, and T-type current, respectively, calculated for the different compartments.

with the contribution of dendritic I_T being negligible. This accounts for the apparent independence of the I_T contribution and EPSC amplitude: the contribution from each spine depends mostly on the strength of its own synaptic input (and of course any variations in the number of calcium channels) and is influenced little by the activity of other synapses. The high spine neck resistance leads different strength synapses to exhibit strongly variable behaviour with respect to T-type channel activation and inactivation. The weaker synapses are unable to activate T-type channels initially or at all, whereas stronger synapses activate a strong I_T component that inactivates quite rapidly during trains. It is only when a variety of different waveforms are combined that the relatively 'proportional' I_T contribution to the compound EPSC train is observed. Our model also suggests that the contribution of any T-type channels in dendrites and in inactive spines will be negligible during sparse synaptic input.

Discussion

A significant I_T-dependent component in PF-PC synaptic responses

Applying a selective antagonist of Ca_V3 channels (Shipe *et al.* 2008), we showed that an I_T-dependent component accounted for 20% of the compound EPSC at PF-PC synapse. By changing holding potentials and by using mutant mice (Figs 2 and 3), we showed this contribution to be exclusively postsynaptic. Although Ca^{2+} measurements in spines and dendrites of PCs have indicated the presence there of T-type calcium channels (Hildebrand *et al.* 2009), our results enable an electrophysiological quantification of this ionic component. Although a synaptic component clearly depends upon I_T, it is difficult to exclude the possibility that I_T might trigger activation of additional conductances that could contribute to the observed effect. These could be triggered by Ca^{2+} influx, such as Ca^{2+}-activated potassium conductances (Engbers *et al.* 2012), or by depolarization, such as P-type calcium channels (Usowicz *et al.* 1992; Kulik *et al.* 2004) or even sodium channels (Vetter *et al.* 2001).

I_T activation in response to a single stimulus

Our recordings were carried out in contrast to most previous studies of T-type channels at near physiological temperature, which results in an ∼3-fold accelerated T-type channel activation/deactivation compared to values measured at room temperature, either in PCs (Isope & Murphy 2005) or, similarly, in expression systems (Iftinca *et al.* 2006). These changes enable T-type channels to respond on a synaptic time scale.

Activation of T-type channels generally requires a combination of hyperpolarization, to relieve steady-state inactivation, and depolarization to activate the channels. Our studies were all carried out from a relatively hyperpolarized potential and therefore only address the activation part of this combination. What cellular events could provide a hyperpolarization? Although PCs usually operate at quite depolarized potentials and fire tonically (Eccles *et al.* 1967), this firing has been reported to hyperpolarize dendrites (Rancz & Häusser 2007). A hyperpolarization can also be caused by a number of potassium conductances expressed in dendrites that can be activated by voltage or second messengers (Canepari & Ogden 2006), although the precise events that could lead to long-lasting hyperpolarizations in dendrites have not been well characterized. One possibility is the pause following the complex spike (Latham & Paul 1971), when a calcium-activated conductance will probably open. Another possibility is during down states of 'bistable' alternations of firing and quiescent phases (Loewenstein *et al.* 2005; but see also Schonewille *et al.* 2006). Perhaps the most obvious source of hyperpolarization is synaptic inhibition; periods of raised activity of the presynaptic basket and stellate cells can certainly silence a PC and drive its membrane potential towards the chloride equilibrium potential (Chavas & Marty, 2003).

From a hyperpolarized potential sufficient to deinactivate 20% of T-type channels, quite a large depolarization is required to activate T-type channels significantly; at least 20 mV according to our experiments imposing EPSP waveforms (Fig. 6*A*). We note, however, that this comparison assumes that T-type calcium channels in the synaptic experiments have the same properties as those characterized biophysically in the young. The subsequent modelling (Fig. 8) employing our biophysical and kinetic characterization of the native T-type channels (Fig. 7) indicated that attaining such depolarizations is non-trivial during sparse synaptic activity. Indeed, the modelling of Roth & Häusser (2001) suggests that such depolarizations will not occur in dendrites (spiny branchlets). We therefore postulated the existence of a strong depolarization of the spine head during synaptic activity. Such depolarization would be caused by the voltage drop accompanying synaptic AMPAR current flow across the spine neck resistance. Sufficient depolarization would, however, require a value of spine neck resistance of the order of 1 GΩ, a value well in excess of the unique (if preliminary) determination of 44 MΩ at PF-contacted PC spines (Roth & Häusser, 2001). It is worth noting that the determination of these high resistances during patch-clamp recordings will depend on the use of pipette solutions with near-physiological

resistivities. Similarly high neck resistances have been reported in other cells (Segev & Rall 1988; Bloodgood & Sabatini 2005; Araya *et al.* 2006; Grunditz *et al.* 2008) and several studies describe synaptic EPSPs that relieve Mg^{2+} block of NMDA receptors or activate voltage-gated calcium channels specifically in spines, which could only be achieved by a strong local depolarization (Denk *et al.* 1995; Yuste *et al.* 1999; Ngo-Anh *et al.* 2005; Grunditz *et al.* 2008; Abrahamsson *et al.* 2012). It should be noted, however, that not all studies found high spine neck resistances (Svoboda *et al.* 1996) and there appears to be quite a wide range of possible values; it has also been reported that the neck resistance can be regulated (Tonnesen *et al.* 2014).

If we accept that the synaptically activated I_T arises exclusively in spines during sparse activity, this provides an explanation for the surprising result that the fractional contribution of I_T to synaptic responses was independent of the response amplitude and input density. Under such conditions, the dendritic depolarization would be negligible compared to the depolarization in active spines. Each spine would therefore recruit I_T independently, allowing linear summation of synaptic responses and of their I_T contributions, with preservation of the proportionality observed with GCL and ML stimulations as well.

If synaptic activation of T-type channels depends on the synaptic current flowing across the spine neck resistance, different synaptic currents would depolarize spines to different extents and thus differentially recruit T-type channels. As expected, in our modelling, only strong synapses were able to activate T-type channels, with the maximum contribution approaching 30% (Fig. 8*C*), with even greater recruitment possible from more hyperpolarized potentials. This suggests the existence of very different calcium signalling between strong and weak synapses, as reported in other neurons (Grunditz *et al.* 2008). Thus, weak and silent synapses reported by Isope & Barbour (2002) will be Ca^{2+} silent, rendering them resistant to Ca^{2+}-dependent synaptic modifications unless there is a strong coincident activation of mGluR1 receptors or a climbing fibre input (Ostu *et al.* 2014). As we showed in the present study, a climbing fibre input is able to depolarize the whole dendritic tree, including PF spines, to the levels required to activate T-type channels.

I_T activation in response to repetitive stimulation

Synaptic T-type channel recruitment represented a relatively constant fraction of EPSC/Ps during repetitive stimulation. Specifically, when we applied pairs of stimuli, we found that the I_T/EPSC ratio remained nearly constant across both responses, independently of the interval between the paired pulses (Figs 4 and 5). This was surprising because T-type channels exhibit rapid voltage-dependent inactivation. The modality of T-channel recruitment in spines and the biophysical properties that we have determined (Fig. 7) offer two mechanisms for the apparently constant synaptic T-channel contribution. First, in spines, spine depolarization would only last as long as the synaptic current, which would be much briefer than the associated dendritic EPSP. The rapidity of the spine repolarization would ensure that a significant fraction of channels would deactivate rather than undergo inactivation and therefore remain available for recruitment during subsequent synaptic responses. The plausibility of this mechanism is demonstrated in Fig. 6 where we imposed a variety of simulated EPSP waveforms and recorded the resulting I_T.

The second explanation for the maintainance of I_T during repetitive stimulation arises from the heterogeneity of synaptic strength and the consequent differences of I_T recruitment. In Fig. 8, weak synapses are unable to recruit I_T at the initial response, requiring paired-pulse facilitation (Fig. 8; see also data with respect to Fig. 6). By contrast, stronger synapses recruit I_T most strongly at the first pulse, whereas it decreases at subsequent pulses as a result of inactivation. When the predicted responses of synapses of different weights were summed according to the reported weights distribution (Brunel *et al.* 2004), a surprisingly constant fraction of repetitive responses was contributed by T-type channels (Fig. 8). The apparently constant fraction of synaptic responses carried by T-type channels may therefore be somewhat misleading, obscuring quite significant variations in I_T amplitude and temporal behaviour between synapses of different weights.

Spine Ca^{2+} entry mediated by I_T

Several sources of calcium have been reported in PF-PC spines (Denk *et al.* 1995). A complex metabotropic pathway is activated upon repetitive PF and/or CF stimulation, involving both a Gαq/Gα11 route with possible inositol trisphosphate receptor activation and, in parallel, a non-selective cationic channel with the development of a slow EPSP (for the first pathway: Finch & Augustine, 1998; Takechi *et al.* 1998; Wang *et al.* 2000; for the latter: Canepari & Ogden, 2006; Hartmann *et al.* 2008). Our recent work (Isope & Murphy, 2005; Hildebrand *et al.* 2009; Otsu *et al.* 2014) and the results of the present study show that T-type channels constitute an additional source of Ca^{2+} in active spines. The contribution of these voltage-dependent channels to intracellular Ca^{2+} dynamics will be controlled in a complex manner by the recent voltage history of PC. T-type VDCCs

can be controlled downstream of mGluR1 activity and could therefore also be tuned by presynaptic activity. Because Ca^{2+} entry through T-type VDCCs can play a role in controlling synaptic plasticity at PF-PC synapses (Ly *et al.* 2013, the complex voltage-dependent and second messenger mechanisms controlling T-type channel recruitment would then contribute to the definition of specific and complex synaptic plasticity rules that depend on both pre- and post-synaptic activity patterns.

Appendix: equations employed in the PC model

T-type channel biophysical characteristics.

$$\tau_m = \left(\frac{1.84}{1+\exp\left(\frac{-0.027-V}{0.008}\right)} + \frac{1.19}{1+\exp\left(\frac{-0.072-V}{-0.020}\right)} \right)^{-1}$$

For $V < -60$ mV, we fitted all the data with the inverse of the sum of two Boltzmann functions.

$$\tau_h = \left(0.0076 + \frac{0.177}{1+\exp\left(\frac{-0.0566-V}{0.0063}\right)} + \frac{0.134}{1+\exp\left(\frac{-0.0995-V}{-0.0056}\right)} \right)^{-1}$$

For $V > -60$ mV, we fitted only the inactivation time constant with the sum two of Boltzmann functions to describe the concavity around –50 mV.

$$\tau_h = \left(3.10 + \frac{3.683}{1+\exp\left(\frac{-0.0379-V}{0.0047}\right)} + \frac{46.34}{1+\exp\left(\frac{-0.0706-V}{-0.0086}\right)} \right)^{-1}$$

τ_h and τ_m are expressed in second

$$m_\infty = \left(\frac{1}{1+\exp\left(\frac{-0.047-V}{0.005}\right)} \right)$$

$$h_\infty = \left(\frac{1}{1+\exp\left(\frac{-0.080-V}{-0.006}\right)} \right)$$

Parameters used in the PC model		
$G_{T,spine}$	2 nS	Spine T-type channel conductance ; adjusted to reproduce observed fraction of EPSC
G_{AMPA}		Spine AMPAR conductances were constrained by the distribution of unitary synaptic charges (Isope and Barbour, 2002); the product of this conductance and the synaptic time constant gives the charge
τ_{off}	1 ms	Decay time constant of synaptic conductance; adjustment described in the Results
$G_{T,dendritic}$	2 μS	Dendrite T-type channel conductance (before division of dendritic compartment)
G_{leak}	100 nS	Global Leak conductance; estimated from recordings
E_{ca}	+45 mV	T-type channel reversal potential
E_{leak}	V_h	Reversal potential fixed to the holding potential
C_{spine}	7.7 fF	Capacitance of the spine; calculated from the geometry reported by Harris & Stevens (1988), assuming 1 μF cm^{-2}
C_d	700 pF	Dendritic capacitance from Roth & Häusser (2001)
C_{so}	29.9 pF	Soma and smooth dendrite capacitance from Roth & Häusser (2001)
$R_{spine\ neck}$	900 MΩ	Spine neck resistance; obtained from fitting model to observations
R_d	6.6 MΩ	Soma to dendritic compartment resistance before division of dendritic compartment (Llano, Marty, Armstrong & Konnerth, 1991)
R_e	7.5 MΩ	Electrode resistance (voltage clamp model)
δ	0.01	Active dendritic fraction, adjusted so that active dendrite had slightly larger unitary EPSP than in Roth and Häusser (2001)

.

References

Abrahamsson T, Cathala L, Matsui K, Shigemoto R & Digregorio DA (2012). Thin dendrites of cerebellar interneurons confer sublinear synaptic integration and a gradient of short-term plasticity. *Neuron* **73**, 1159–1172.

Araya R, Jiang J, Eisenthal KB & Yuste R (2006). The spine neck filters membrane potentials. *Proc Natl Acad Sci USA* **103**, 17961–17966.

Astori S, Wimmer RD, Prosser HM, Corti C, Corsi M, Liaudet N, Volterra A, Franken P, Adelman JP & Lüthi A (2011). The Cav3.3 calcium channel is a major sleep spindle pacemaker in thalamus. *Proc Natl Acad Sci USA* **108**, 13823–13828.

Barbour B, Keller BU, Llano I & Marty A (1994). Prolonged presence of glutamate during excitatory synaptic transmission to cerebellar Purkinje cells. *Neuron* **12**, 1331–1343.

Batchelor AM, Magde DJ & Garthwaite J (1994). Synaptic activation of metabotropic glutamate receptors in the parallel fibre-Purkinje cell pathway in rat cerebellar slices. *Neuroscience* **63**, 911–915.

Bloodgood BL & Sabatini BL (2005). Neuronal activity regulates diffusion across the neck of dendritic spines. *Science* **310**, 866–869.

Bossu JL, Fagni L & Feltz A (1989). Voltage-activated calcium channels in rat Purkinje cells maintained in culture. *Pflügers Arch* **414**, 92–94.

Brenowitz SD & Regehr WG (2005). Associative short-term synaptic plasticity mediated by endocannabinoids. *Neuron* **45**, 419–431.

Brown SP, Safo PK & Regehr WG (2004). Endocannabinoids inhibit transmission at granule cell to Purkinje cell synapses by modulating three types of presynaptic calcium channels. *J Neurosci* **24**, 5623–5631.

Brunel N, Hakim V, Isope P, Nadal JP & Barbour B (2004). Optimal information storage and the distribution of synaptic weights: perceptron versus Purkinje cell. *Neuron* **43**, 745–757.

Burgess DE, Crawford O, Delisle BP & Satin J (2002). Mechanism of inactivation gating of human T-type (low-voltage activated) calcium channels. *Biophys J* **82**, 1894–1906.

Canepari M & Ogden D (2006). Kinetic, pharmacological and activity-dependent separation of two Ca^{2+} signalling pathways mediated by type 1 metabotropic glutamate receptors in rat Purkinje neurones. *J Physiol* **573**, 65–82.

Chadderton P, Margrie TW & Häusser M (2004) Integration of quanta in cerebellar granule cells during sensory processing. *Nature* **428**, 856–860.

Chavas J & Marty A (2003). Coexistence of excitatory and inhibitory GABA synapses in the cerebellar interneuron network. *J Neurosci* **23**, 2019–2031.

Coesmans M, Weber JT, De Zeeuw CI & Hansel C (2004). Bidirectional parallel fiber plasticity in the cerebellum under climbing fiber control. *Neuron* **44**, 691–700.

Daniel H, Levenes C & Crepel F (1998). Cellular mechanisms of cerebellar LTD. *Trends Neurosci* **21**, 401–407.

Denk W, Sugimori M & Llinas R (1995). Two types of calcium response limited to single spines in cerebellar Purkinje cells. *Proc Natl Acad Sci USA* **92**, 8279–8282.

Dreyfus FM, Tscherter A, Errington AC, Renger JJ, Shin HS, Uebele VN, Crunelli V, Lambert RC & Leresche N (2010). Selective T-type calcium channel block in thalamic neurons reveals channel redundancy and physiological impact of I(T)window. *J Neurosci* **30**, 99–109.

Dugue GP, Dumoulin A, Triller A & Dieudonne S (2005). Target-dependent use of co-released inhibitory transmitters at central synapses. *J Neurosci* **25**, 6490–6498.

Eccles JC, Ito M & Szentagothai J (1967). *The Cerebellum as a Neuronal Machine*. Springer-Verlag, Berlin; p. 343.

Engbers JD, Anderson D, Asmara H, Rehak R, Mehaffey WH, Hameed S, McKay BE, Kruskic M, Zamponi GW & Turner RW (2012). Intermediate conductance calcium-activated potassium channels modulate summation of parallel fiber input in cerebellar Purkinje cells. *Proc Natl Acad Sci USA* **109**, 2601–2606.

Finch EA & Augustine GJ (1998). Local calcium signalling by inositol-1,4,5-trisphosphate in Purkinje cell dendrites. *Nature* **396**, 753–756.

Grunditz A, Holbro N, Tian L, Zuo Y & Oertner TG (2008). Spine neck plasticity controls postsynaptic calcium signals through electrical compartmentalization. *J Neurosci* **28**, 13457–13466.

Harris KM & Stevens JK (1988). Dendritic spines of rat cerebellar Purkinje cells: serial electron microscopy with reference to their biophysical characteristics. *J Neurosci* **8**, 4455–4469.

Hartmann J & Konnerth A (2005). Determinants of postsynaptic Ca^{2+} signaling in Purkinje neurons. *Cell Calcium* **37**, 459–466.

Hartmann J, Dragicevic E, Adelsberger H, Henning HA, Sumser M, Abramowitz J, Blum R, Dietrich A, Freichel M, Flockerzi V, Birnbaumer L & Konnerth A (2008). TRPC3 channels are required for synaptic transmission and motor coordination. *Neuron* **59**, 392–398.

Häusser M & Roth A (1997). Dendritic and somatic glutamate receptor channels in rat cerebellar Purkinje cells. *J Physiol* **501**, 77–95.

Hildebrand ME, Isope P, Miyazaki T, Nakaya T, Garcia E, Feltz A, Schneider T, Hescheler J, Kano M, Sakimura K, Watanabe M, Dieudonne S & Snutch TP (2009). Functional coupling between mGluR1 and Cav3.1 T-type calcium channels contributes to parallel fiber-induced fast calcium signaling within Purkinje cell dendritic spines. *J Neurosci* **29**, 9668–9682.

Iftinca M, McKay BE, Snutch TP, McRory JE, Turner RW & Zamponi GW (2006). Temperature dependence of T-type calcium channel gating. *Neuroscience* **142**, 1031–1042.

Isope P & Barbour B (2002). Properties of unitary granule cell→Purkinje cell synapses in adult rat cerebellar slices. *J Neurosci* **22**, 9668–9678.

Isope P & Murphy TH (2005). Low threshold calcium currents in rat cerebellar Purkinje cell dendritic spines are mediated by T-type calcium channels. *J Physiol* **562**, 257–269.

Jorntell H & Ekerot CF (2006). Properties of somatosensory synaptic integration in cerebellar granule cells in vivo. *J Neurosci* **26**, 11786–11797.

Kulik A, Nakadate K, Hagiwara A, Fukazawa Y, Lujan R, Saito H, Suzuki N, Futatsugi A, Mikoshiba K, Frotscher M & Shigemoto R (2004). Immunocytochemical localization of the alpha 1A subunit of the P/Q-type calcium channel in the rat cerebellum. *Eur J Neurosci* **19**, 2169–2178.

Lambolez B, Audinat E, Bochet P, Crepel F & Rossier J (1992). AMPA receptor subunits expressed by single Purkinje cells. *Neuron* **9**, 247–258.

Latham A & Paul DH (1971). Spontaneous activity of cerebellar Purkinje cells and their responses to impulses in climbing fibres. *J Physiol* **213**, 135–156.

Llano I, Marty A, Armstrong CM & Konnerth A (1991). Synaptic- and agonist-induced excitatory currents of Purkinje cells in rat cerebellar slices. *J Physiol* **434**, 183–213.

Llinas R & Sugimori M (1980). Electrophysiological properties of in vitro Purkinje cell dendrites in mammalian cerebellar slices. *J Physiol* **305**, 197–213.

Loewenstein Y, Mahon S, Chadderton P, Kitamura K, Sompolinsky H, Yarom Y & Hausser M (2005). Bistability of cerebellar Purkinje cells modulated by sensory stimulation. *Nat Neurosci* **8**, 202–211.

Ly R, Bouvier G, Schonewille M, Arabo A, Rondi-Reig L, Lena C, Casado M, De Zeeuw CI & Feltz A (2013). T-type channel blockade impairs long-term potentiation at the parallel fiber-Purkinje cell synapse and cerebellar learning. *Proc Natl Acad Sci USA* **110**, 20302–20307.

Masugi-Tokita M, Tarusawa E, Watanabe M, Molnar E, Fujimoto K & Shigemoto R (2007). Number and density of AMPA receptors in individual synapses in the rat cerebellum as revealed by SDS-digested freeze-fracture replica labeling. *J Neurosci* **27**, 2135–2144.

McKay BE & Turner RW (2005). Physiological and morphological development of the rat cerebellar Purkinje cell. *J Physiol* **567**, 829–850.

McKay BE, McRory JE, Molineux ML, Hamid J, Snutch TP, Zamponi GW & Turner RW (2006). Ca(V)3 T-type calcium channel isoforms differentially distribute to somatic and dendritic compartments in rat central neurons. *Eur J Neurosci* **24**, 2581–2594.

Mintz IM, Sabatini BL & Regehr WG (1995). Calcium control of transmitter release at a cerebellar synapse. *Neuron* **15**, 675–688.

Misra C, Brickley SG, Farrant M & Cull-Candy SG (2000). Identification of subunits contributing to synaptic and extrasynaptic NMDA receptors in Golgi cells of the rat cerebellum. *J Physiol* **524**, 147–162.

Momiyama A, Feldmeyer D & Cull-Candy SG (1996). Identification of a native low-conductance NMDA channel with reduced sensitivity to Mg^{2+} in rat central neurones. *J Physiol* **494**, 479–492.

Mouginot D, Bossu JL & Gähwiler BH (1997). Low-threshold Ca^{2+} currents in dendritic recordings from Purkinje cells in rat cerebellar slice cultures. *J Neurosci* **17**, 160–170.

Myoga MH & Regehr WG (2011). Calcium microdomains near R-type calcium channels control the induction of presynaptic long-term potentiation at parallel fiber to purkinje cell synapses. *J Neurosci* **31**, 5235–5243.

Ngo-Anh TJ, Bloodgood BL, Lin M, Sabatini BL, Maylie J & Adelman JP (2005). SK channels and NMDA receptors form a Ca^{2+}-mediated feedback loop in dendritic spines. *Nat Neurosci* **8**, 642–649.

Otsu Y, Marcaggi P, Feltz A, Isope P, Kollo M, Nusser Z, Mathieu B, Kano M, Tsujita M, Sakimura K & Dieudonne S (2014). Activity-dependent gating of calcium spikes by A-type K^+ channels controls climbing fiber signaling in Purkinje cell dendrites. *Neuron* **84**, 137–151.

Petrenko AB, Tsujita M, Kohno T, Sakimura K & Baba H (2007). Mutation of alpha1G T-type calcium channels in mice does not change anesthetic requirements for loss of the righting reflex and minimum alveolar concentration but delays the onset of anesthetic induction. *Anesthesiology* **106**, 1177–1185.

Rancz EA & Häusser M (2006). Dendritic calcium spikes are tunable triggers of cannabinoid release and short-term synaptic plasticity in cerebellar Purkinje neurons. *J Neurosci* **26**, 5428–5437.

Rancz EA & Häusser M (2007). Somatic firing hyperpolarizes Purkinje dendrites. *Soc Neurosci Abstr*, p 251.210.

R Development Core Team (2011). *R: A language and environment for statistical computing*. R Foundation for Statistical Computing, Vienna.

Rosenmund C, Legendre P & Westbrook GL (1992). Expression of NMDA channels on cerebellar Purkinje cells acutely dissociated from newborn rats. *J Neurophysiol* **68**, 1901–1905.

Roth A & Häusser M (2001). Compartmental models of rat cerebellar Purkinje cells based on simultaneous somatic and dendritic patch-clamp recordings. *J Physiol* **535**, 445–472.

Schonewille M, Khosrovani S, Winkelman BH, Hoebeek FE, De Jeu MT, Larsen IM, Van der Burg J, Schmolesky MT, Frens MA & De Zeeuw CI (2006). Purkinje cells in awake behaving animals operate at the upstate membrane potential. *Nat Neurosci* **9**, 459–461.

Segev I & Rall W (1988). Computational study of an excitable dendritic spine. *J Neurophysiol* **60**, 499–523.

Shipe WD, Barrow JC, Yang ZQ, Lindsley CW, Yang FV, Schlegel KA, Shu Y, Rittle KE, Bock MG, Hartman GD, Tang C, Ballard JE, Kuo Y, Adarayan ED, Prueksaritanont T, Zrada MM, Uebele VN, Nuss CE, Connolly TM, Doran SM, Fox SV, Kraus RL, Marino MJ, Graufelds VK, Vargas HM, Bunting PB, Hasbun-Manning M, Evans RM, Koblan KS & Renger JJ (2008). Design, synthesis, and evaluation of a novel 4-aminomethyl-4-fluoropiperidine as a T-type Ca^{2+} channel antagonist. *J Med Chem* **51**, 3692–3695.

Soetaert K, Petzoldt T & Setzer RW (2010). Solving differential equation in R: Package deSolve. *Journal of Statistical Software* **33**, 1–25.

Svoboda K, Tank DW & Denk W (1996). Direct measurement of coupling between dendritic spines and shafts. *Science* **272**, 716–719.

Takechi H, Eilers J & Konnerth A (1998). A new class of synaptic response involving calcium release in dendritic spines. *Nature* **396**, 757–760.

Talley EM, Cribbs LL, Lee JH, Daud A, Perez-Reyes E & Bayliss DA (1999). Differential distribution of three members of a gene family encoding low voltage-activated (T-type) calcium channels. *J Neurosci* **19**, 1895–1911.

Tonnesen J, Katona G, Rozsa B & Nagerl UV (2014). Spine neck plasticity regulates compartmentalization of synapses. *Nat Neurosci* **17**, 678–685.

Usowicz MM, Sugimori M, Cherksey B & Llinas R (1992). P-type calcium channels in the somata and dendrites of adult cerebellar Purkinje cells. *Neuron* **9**, 1185–1199.

Valera AM, Doussau F, Poulain B, Barbour B & Isope P (2012). Adaptation of granule cell to Purkinje cell synapses to high-frequency transmission. *J Neurosci* **32**, 3267–3280.

Vetter P, Roth A & Häusser M (2001). Propagation of action potentials in dendrites depends on dendritic morphology. *J Neurophysiol* **85**, 926–937.

Wang SS, Denk W & Hausser M (2000). Coincidence detection in single dendritic spines mediated by calcium release. *Nat Neurosci* **3**, 1266–1273.

Westenbroek RE, Sakurai T, Elliott EM, Hell JW, Starr TV, Snutch TP & Catterall WA (1995). Immunochemical identification and subcellular distribution of the alpha 1A subunits of brain calcium channels. *J Neurosci* **15**, 6403–6418.

Yuste R, Majewska A, Cash SS & Denk W (1999). Mechanisms of calcium influx into hippocampal spines: heterogeneity among spines, coincidence detection by NMDA receptors, and optical quantal analysis. *J Neurosci* **19**, 1976–1987.

Additional information

Competing interests

The authors declare that they have no competing interests.

Funding

RL was successively supported by a 3 year CNRS BDI fellowship and a 1 year FRM/Université Pierre et Marie Curie (UPMC) fellowship. GB was supported by the Fondation pour la Recherche Médicale. This work was supported by CNRS, ANR (ANR-09-MNPS-038-03, ANR-08-SYSC-005, ANR-2010-JCJC-1403-01). This work has also received support under the program 'Investissements d'Avenir' launched by the French Government and implemented by the ANR, with the references: ANR-10-LABX-54 MEMO LIFE and ANR-11-IDEX-0001-02 PSL* Research University.

Author contributions

RL, PI, BB and AF designed the experiments. MK and KS provided the $Ca_V3.1$ KO mice. AR provided access to the $CA_V3.3$ mice that he had developed with HP. RL carried out the electrophysiology experiments and analysis, except for Fig. 2I, which was contributed by GB and GS. RL and BB developed the modelling. All authors contributed to the manuscript. All authors have approved the final version of the manuscript and agree to be accountable for all aspects of the work. All persons designated as authors qualify for authorship, and all those who qualify for authorship are listed.

Acknowledgements

We want to specially thank Victor N. Uebele and John J. Renger from Merck Research Labs who provided us with TTA-P2, a specific Ca_V3 antagonist at a time when it was not commercially available and with related pharmacological data. Only their employer's policies prevent their authorship with respect to the present paper.